



Permafrost Monitoring from Space

Annett Bartsch¹  · Tazio Strozzi² · Ingmar Nitze³

Received: 2 August 2022 / Accepted: 26 January 2023 / Published online: 14 March 2023
© The Author(s) 2023

Abstract

Permafrost is a sub-ground phenomenon and therefore cannot be directly observed from space. It is an Essential Climate Variable and associated with climate tipping points. Multi-annual time series of permafrost ground temperatures can be, however, derived through modelling of the heat transfer between atmosphere and ground using landsurface temperature, snow- and landcover observations from space. Results show that the northern hemisphere permafrost ground temperatures have increased on average by about one degree Celsius since 2000. This is in line with trends of permafrost proxies observable from space: surface water extent has been decreasing across the Arctic; the landsurface is subsiding continuously in some regions indicating ground ice melt; hot summers triggered increased subsidence as well as thaw slumps; rock glaciers are accelerating in some mountain regions. The applicability of satellite data for permafrost proxy monitoring has been demonstrated mostly on a local to regional scale only. There is still a lack of consistency of acquisitions and of very high spatial resolution observations. Both are needed for implementation of circumpolar monitoring of lowland permafrost. In order to quantify the impacts of permafrost thaw on the carbon cycle, advancement in wetland and atmospheric greenhouse gas concentration monitoring from space is needed.

Keywords Permafrost · Thaw · Arctic · Mountains · Satellite · Time series

Tazio Strozzi and Ingmar Nitze have contributed equally to this work.

 Annett Bartsch
annett.bartsch@bgeos.com

Tazio Strozzi
strozzi@gamma-rs.ch

Ingmar Nitze
ingmar.nitze@awi.de

¹ b.geos, Industriestrasse 1, 2100 Korneuburg, Austria

² Gamma Remote Sensing, Worbstrasse 225, 3073 Gümligen, Switzerland

³ Alfred Wegener Institute, Helmholtz Centre for Polar and Marine Research, Telegrafenberg A 45, 14473 Potsdam, Germany

Article Highlights

- Trends from modelling results using landsurface temperature agree with a multitude of proxies observable from space
- Different proxies from observations since 2000 indicate widespread permafrost thaw across the Arctic and in mountains
- Understanding the implications of thawing permafrost is expected to advance with enhanced data availability and products

1 Introduction

Permafrost is an Essential Climate Variable (ECV; Global Climate Observing System GCOS (2016)). It is ground (soil or rock and included ice and organic material) that remains at or below zero degree Celsius for at least two consecutive years (Van Everdingen et al. 1998). Permanently frozen ground can be found under 15% of the Northern Hemisphere's exposed landsurface (Obu 2021). The area affected by permafrost increases to about 22 % when allowing discontinuities in distribution (commonly referred to as permafrost extent). In situ observations from boreholes show that ground temperatures are steadily increasing (Biskaborn et al. 2019) which leads to degradation in transition zones. Permafrost thaw in high latitude lowlands is of specific concern due to storage of substantial amounts of carbon in the soils (Schuur et al. 2015; Miner et al. 2022). Ground ice melt is expected to trigger the release of methane (CH_4) and carbon dioxide (CO_2), which leads to further warming at the global scale and therefore potentially further permafrost thaw (Schuur et al. 2015). The release is considered the key impact of permafrost tipping (Lenton et al. 2008; Swingedouw et al. 2020). Gradual permafrost thaw, permafrost collapse through internal heat production as well as abrupt thaw on a local scale are distinguished in this context (McKay et al. 2022). Monitoring thaw as well as carbon cycle impacts is challenging with respect to in situ as well as remote observations. In situ observation of permafrost state on a global scale requires the establishment of borehole networks in a representative distribution what is currently not feasible (Biskaborn et al. 2015). Remote sensing is limited to surface expressions. Monitoring needs to address key parameters for permafrost and should also consider others from space-observable indicators. These include especially rock glacier kinematics for mountainous regions and a range of surface expressions in lowland area (e.g. thaw lake dynamics, thaw subsidence and mass movements). This overview article reviews types of satellite data and methods which can contribute to (1) the assessment of sub-ground conditions and, specifically, key parameters, and (2) monitoring of environmental impact of thaw. In the latter case, both lowland and mountain permafrost (rock glaciers) are discussed. First, key parameters are introduced, then observation capabilities discussed and eventually information gained through space-borne remote sensing is summarized.

2 Key Parameters and Monitoring Requirements

Parameters which are historically considered as essential for permafrost monitoring by GCOS are ground temperature and active layer thickness. The ground surface thaws during the unfrozen period, which is referred to as the active layer. It reaches its maximum towards the end of the thaw season (active layer thickness—ALT) and can range from

decimetres to metres. Sub-ground temperature as well as active layer thickness cannot be directly captured with remote sensing. The ECV Permafrost has therefore not been listed as ‘space-observable’ by GCOS (2016). Measurement accuracy requirements are thus so far formulated only with respect to in situ measurements. GCOS (2021) notes that current space-based approaches do not meet these requirements. The monitoring of related surface features in mountain areas (kinematics of rock glaciers) and terrain changes in lowlands (subsidence as property of the active layer) are, however, recommended for further investigation with satellite data. Rock glacier kinematics have been added recently to the GCOS list of ECV Permafrost key parameters (GCOS 2022).

Nevertheless, modelling of ground temperature using partially parameters observable from space (e.g. surface temperature, snow) has been developed over recent years (e.g. Obu et al. 2019; Fig. 1d) as it provides the best option for spatially continuous information. User requirements for gridded products have been collected through (Bartsch et al. (2020b); National Research Council (2014), Tables 1 and 2) to complement the GCOS specifications for in situ measurements. In general at least annual time series are targeted (threshold) representing mean annual ground temperature (MAGT) and maximum depth of the active layer (ALT).

Many applications make use of information on permafrost extent which reflects ground temperature spatial distribution. The measuring unit is defined as % within a grid cell. User requirements for permafrost extent have been reviewed with respect to potential future satellite missions (European Commission. Joint Research Centre. (2018); Table 3). Threshold and goal requirements are also addressed in the WMO OSCAR (World Meteorological Organization Observing systems Capability Analyses and Review Tool) database (Bartsch et al. 2020b). Five days are suggested as the threshold for temporal sampling which deviates considerably from published expert suggestions (annual to decadal sampling, table 3).

A commonly used representation of permafrost extent is the map produced by Brown et al. (1997). The permafrost map covers the northern hemisphere north of about 30°N. It provides a generalized view of pre-1990 s conditions of permafrost fraction classified into four zones. It is commonly referred to as the IPA (International Permafrost Association) map (Fig. 1a) and is widely used. The zones can be also represented through fractions/probabilities of permafrost presence derived from models (e.g. using ground temperature representing 2 m depth, Fig. 1a, d).

3 Assessment of Sub-ground Conditions

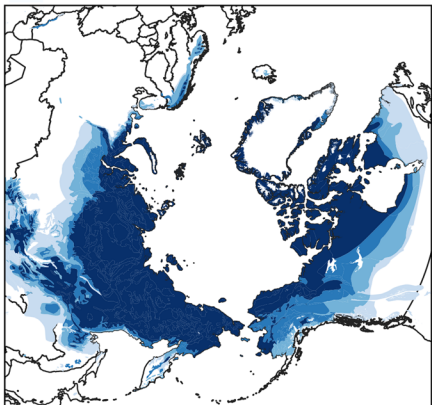
3.1 Drivers and Proxies of Ground Temperature

Models utilize satellite-derived temperature observations from the surface to estimate ground temperature. Such an approach allows the retrieval on global scale (Obu et al. (2019, 2021b); Fig. 1b, d). Landcover information together with snow is of high relevance for heat transfer between the ground and the atmosphere (e.g. Westermann et al. (2017) and Trofaier et al. (2017)). Coefficients, for example, heat capacity and thermal conductivity, are selected according to landcover information (Westermann et al. 2015). Subgrid information on landcover is in addition required for the generation of ensembles of input parameters for permafrost modelling (Langer et al. 2010). Satellite-derived landsurface

a) IPA map based on Brown et al. (1997)

Permafrost zones

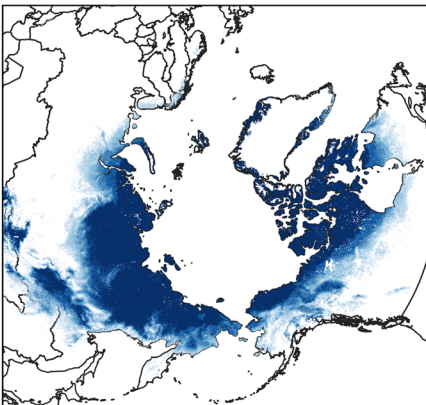
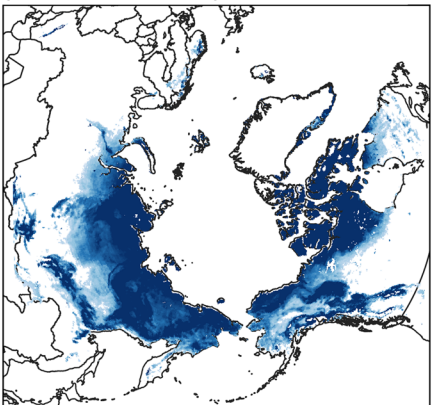
- Continuous
- Discontinuous
- Sporadic
- Isolated



b) Permafrost_cci v2 for 2018 (Obu et al. 2020)

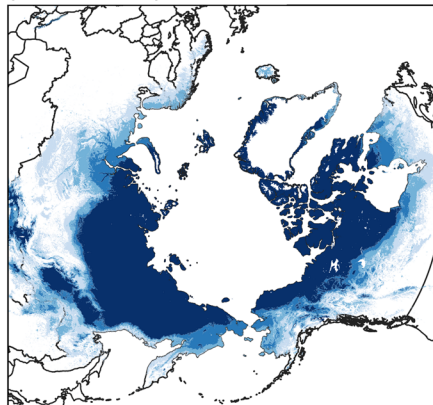
Permafrost fraction in %

- 10
- 50
- 90
- 100

c) MAGT based on surface status 2007-2011
(Kroisleitner et al. 2018)

MAGT in °C

- < -3.5
- -2 - -3.5
- -1 - -2
- 0 - -1

d) GlobPermafrost, 2000-2016
(Obu et al. 2019)

Permafrost zones

- Continuous
- Discontinuous
- Sporadic
- Isolated

Fig. 1 Circumpolar representation of permafrost: **a** permafrost zones based on traditional mapping (Brown et al. 1997), **b** Transient modelling of permafrost fraction using satellite-derived landsurface temperature representing a specific year (Obu et al. 2021b), **c** satellite radar-derived surface status converted to mean annual ground temperature (MAGT) (Kroisleitner et al. 2018) and **d** Equilibrium modelling of permafrost probability converted to permafrost zones using satellite-derived landsurface temperature representing an average of several years (Obu et al. 2019)

Table 1 Requirements for satellite-derived ground temperature (Permafrost_cci; Bartsch et al. (2020b)) versus in situ observations (GCOS 2022). ZAA—Zero Annual Amplitude

	Permafrost_cci requirements		GCOS requirements		
	Threshold	Goal	Threshold	Breakthrough	Goal
Geographical coverage	Pan-Arctic	Global with regional specific products	—	—	—
Temporal sampling	Annually	Monthly	Monthly	Daily	Hourly
Temporal extent	Last decade	1979–present	—	—	—
Horizontal resolution	10 km	1 km	Characterization of bioclimatic zones	Transsects	Regular spacing of boreholes
Subgrid variability	No	Yes	—	—	—
Vertical resolution	50 cm exponential	5 cm exponential	50 cm	—	20 cm
vertical extent	15 m	30 m	Below permafrost table	Down to ZAA	Deeper than ZAA
Accuracy	RMSE < 2.5°C	RMSE < 0.5°C	0.2 °C	0.1 °C	0.01 °C
Stability	Higher stability than existing datasets	Accuracy needs to be temporally homogeneous	0.1 °C	0.05 °C	0.01 °C

Table 2 Requirements for satellite-derived active layer thickness (Permafrost_cci, Bartsch et al. (2020b) and National Research Council (2014)) versus in situ observations (GCOS 2022)

	Permafrost_cci		NRC Target	GCOS requirements		
	Threshold	Target		Threshold	Breakthrough	Goal
Geographical coverage	Pan-Arctic	Global with regional specific products	–	–	–	–
Temporal sampling	< yearly	< monthly	Biweekly	End of thaw period	End of thaw period	–
Temporal extent	Last decade	1979–present	–	–	–	–
Horizontal resolution	10 km	1 km	30 m	Characterization of bioclimatic zone	Transects	Regular spacing of boreholes
Vertical resolution	–	–	5 cm	20 cm	10 cm	2 cm
Precision	10 cm	1 cm	–	–	–	–
Accuracy	RMSE < 25 cm	RMSE < 10 cm	–	2/15 cm*	–	1/5 cm*
Stability	Accuracy needs to be temporally homogeneous	–	10 cm	5 cm	5 cm	1 cm

*Mechanical probing penetration uncertainty/sensor uncertainty

Table 3 Requirements for satellite-derived permafrost extent (European Commission. Joint Research Centre. 2018; National Research Council 2014)

	Threshold	Breakthrough	Goal
Temporal sampling	10 years	–	Annually
Horizontal resolution	100 m	10 m	1 m
Accuracy	85%	–	95%

temperature and landcover have been, for example, used with the permafrost model CryoGRID (Obu et al. 2019). It could be determined that the actual area underlain by permafrost (permafrost area) accounts for approximately 14 million km² (15% of the exposed landsurface area in the Northern Hemisphere) and globally 13.97 km² (11%) (Obu 2021).

Landsurface temperature (LST) datasets based on MODIS (Moderate Resolution Imaging Spectroradiometer) are currently the most frequently used due to good data availability (repeat intervals as well as length of record spanning more than 20 years, products starting 2000). Hachem et al. (2012) found that LST derived from MODIS and daily near-surface air temperatures are comparable. Permafrost applications require continuous records throughout the year. In case of thermal infrared, cloud gap filling is therefore required. Aspects of this issue are discussed in, for example, Hachem et al. (2009) and Westermann et al. (2017). Clear sky bias has been also discussed for MODIS as well as Advanced Along-Track Scanning Radiometer (AATSR) LST products in comparison with passive microwave skin temperatures derived from the Advanced Microwave Scanning Radiometer for EOS (AMSR-E) and Special Sensor Microwave/Imager (SSM/I) data (Soliman et al. 2012). Passive microwave records can to some extent provide an alternative (André et al. 2015) but the spatial resolution is much coarser. While infrared-derived products are in the order of 1 km or better, passive microwave information represents several tens of kilometres. A practical solution is the combination of infrared products with climate reanalysis data to obtain spatially and temporal continuous records (Westermann et al. 2017). Reanalyses data are used for gap filling MODIS LST. MODIS LST can be used for bias correction of reanalyses data which also allows extension of records before availability of MODIS. Retrievals based on annual records by Obu et al. (2021b) starting 1997 (reanalyses data use before 2000 (ERA5), MODIS & ERA5 after 2000) show that ground temperature increase at 2 m depth is highest along the Arctic coastline (Miner et al. 2022). The overall trend for the northern hemisphere follows sea ice decline ($R^2 = 0.75$). The lower the minimum sea ice extent, the higher the temperatures in the ground (Fig. 2). A change of on average one degree Celsius at 2 m depth (referring to the area of permafrost extent maximum within the observation period, 1997–2019) coincides with a September sea ice decline of about 2.5 million km². Continuity of thermal infrared acquisitions at a similar or better level is needed. A service could be potentially provided through Copernicus Sentinel missions (e.g. Sentinel-3 SLSTR).

Microwave records can provide an independent source to evaluate infrared-derived products and, in the case of passive microwave data, they can extent far back in time. Both active and passive sensor types are able to capture near-surface soil status (frozen or unfrozen) due to the sensitivity to dielectric properties. Freeze/thaw information has been shown to be suitable as proxy for sub-ground conditions (Park et al. 2016; Kroisleitner et al. 2018). The number of frozen days per year is summed up and converted to potential ground temperature (empirical model calibrated with borehole in situ measurements—FT2T: Freeze Thaw to Temperature; Fig. 1c). The performance depends on landcover (Bergstedt and Bartsch 2017; Bergstedt et al. 2020a), wavelength (Kroisleitner et al. 2018),

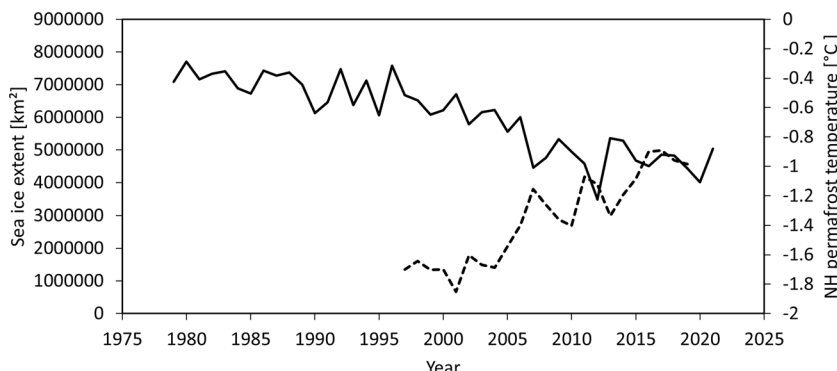


Fig. 2 Northern hemisphere (NH) permafrost temperature change at 2 m depth (dashed line; *source* transient modelling using landsurface temperature (reanalyses data and near infrared (MODIS, 1 km); CryoGRID; Permafrost_cci v3, (Obu et al. 2021b)) compared to sea ice extent for September (solid line; sea ice concentration data from 1979 to 2021 were obtained from <https://www.meereisportal.de> (grant: REKLIM-2013-04, Spreen et al. (2008))

acquisition timing and the algorithm used to derive the surface state. Surface freeze/thaw state is in general defined binary (yes/no), rather than fraction. Current freeze/thaw products aim at identification of an average surface state condition within a footprint or the completion of thaw and start of freeze/up [Kim et al. (2012) using SSMI, Naeimi et al. (2012) using ASCAT, Derksen et al. (2017) using SMAP, Rautiainen et al. (2016) using SMOS]. The average state has been exploited for permafrost mapping purposes (Park et al. 2016; Kroisleitner et al. 2018). Results based on Metop ASCAT (FT2T approach) provide similar results compared to transient modelling using LST (Obu et al. 2021b)) for Russia as well as Canada (Fig. 3). Regions with specifically mountain ranges show larger deviations. In general ASCAT-based MAGT has often a negative bias as the insulating effect of snow is not considered in such an approach.

3.2 Proxies for Active Layer Thickness

In situ, the active layer thickness (ALT) is obtained by probing with metal rods or as derivation of densely distributed thermistors in boreholes. Various techniques have been tested to obtain spatially distributed information from satellite data. Landcover-related information has been frequently used to make assumptions regarding active layer thickness. An empirical relationship is established and maps of potential ALT derived. Investigations have been made using optical as well as microwave satellite data. This includes the analyses of the normalized difference vegetation index (NDVI) (McMichael et al. 1997; Kelley et al. 2004), landcover classes (Nelson et al. 1997; Peddle and Franklin 1993) as well as backscatter amplitude from X-band synthetic aperture radar [SAR; Widhalm et al. (2016, 2017)]. The consideration of derivatives of digital elevation models (DEMs) has been shown to be of added value (Peddle and Franklin 1993; Leverington and Duguay 1996; Gangodagamage et al. 2014). Hyperspectral analyses demonstrated that spectral resolution is important for such applications and even variations from year to year can be captured (Zhang et al. 2021). Properties of the active layer have been also investigated through airborne P-band SAR observations. This included retrieval of soil moisture content

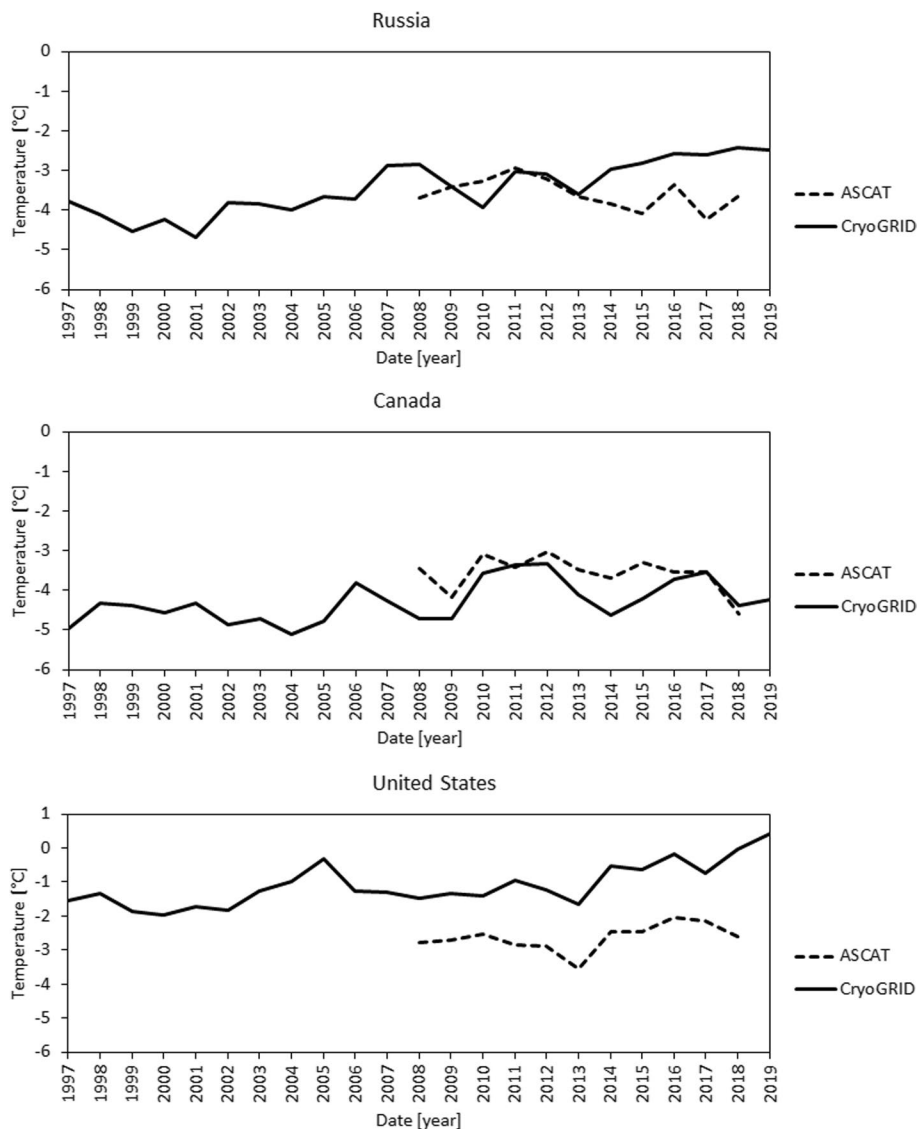


Fig. 3 Regional ground temperature change (1 m depth) in permafrost regions of selected countries: comparison between surface status derived temperature (C-band scatterometer, Metop ASCAT; FT2T; Kroisleitner et al. (2018), corrected for water fraction according to Bergstedt et al. 2020, in situ calibration dataset from Heim et al. (2021)) and transient modelling using landsurface temperature (near infrared, MODIS, 1 km; CryoGRID; Permafrost_cci v3, (Obu et al. 2021b))

as well as active layer thickness (Chen et al. 2019; Parsekian et al. 2021). In the latter case, there are, however, limitations in case of larger depths.

Soils, including the active layer, often contain ice. Ground subsides when this ice melts due to seasonal thaw or long-term changes. These changes are comparably small, in the order of a few centimetres. Especially of relevance as remote sensing technique is SAR

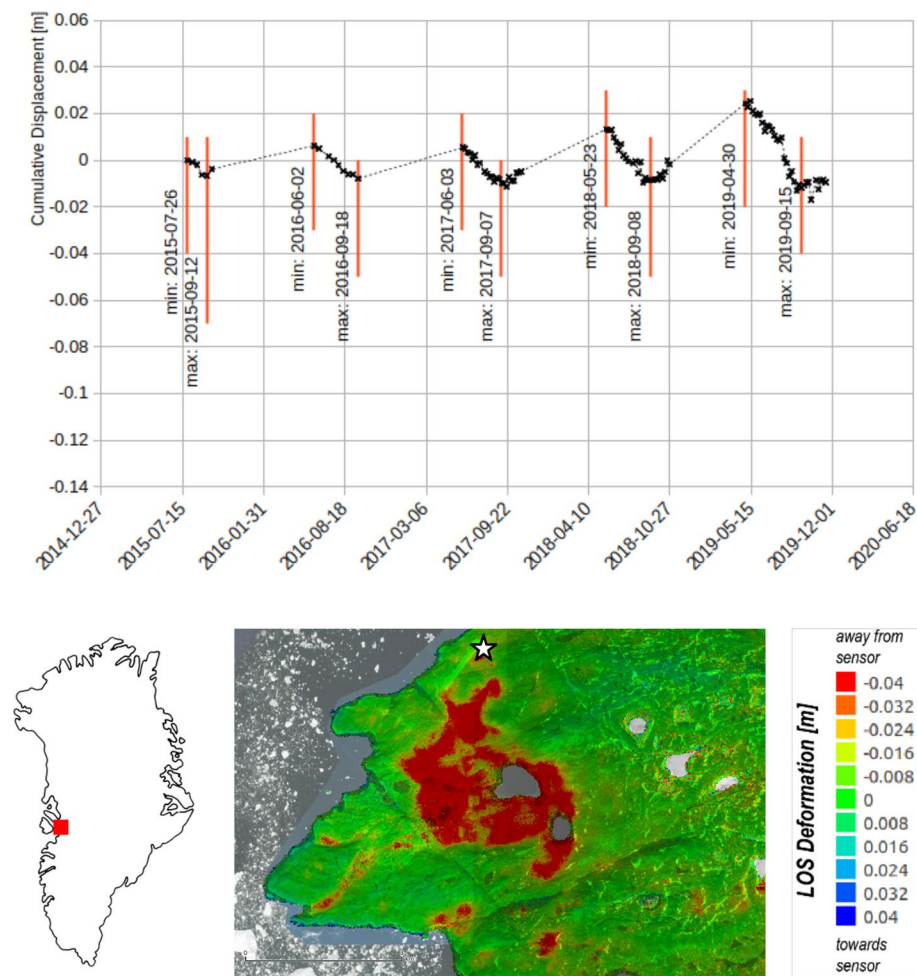


Fig. 4 Subsidence map over Ilulissat (Greenland) from Copernicus Sentinel-1 InSAR from 30 April to 15 September 2019 and time series of displacement in the line-of-sight direction on peat terrain close to the airport (see white star for position). Background map data source: Google, DigitalGlobe

Interferometry (InSAR) as such subtle changes can be detected (e.g. Short et al. 2011; Liu et al. 2012; Rouyet et al. 2019; Strozzi et al. 2018; Fig. 4).

The through InSAR captured seasonal variations in ground displacements are expected to reflect changes in thaw depth and ALT, respectively (Liu et al. 2012). In case that the soil profile is uniform and is fully saturated, ALT can be directly inferred (Schaefer et al. 2015). In other cases, models which reflect the varying soil layer properties and variations in wetness need to be used (e.g. Wang et al. 2018; Zhao et al. 2016). This does, however, require detailed knowledge of the soil stratigraphy, which is rarely available across the Arctic. A further challenge is the limited availability of in situ measurements of subsidence and active layer thickness at the same time. The performance of InSAR as well as different wavelengths has been, for example, assessed with in situ records in a case study for central Yamal, Russia (Bartsch et al. 2019). It could be demonstrated that both X-band and C-band

retrievals agree (1) with each other and (2) with the subsidence magnitude of in situ observations. In addition, a larger annual subsidence is observed for years with higher ALT. A further issue that was raised is the comparability between different years when signal decorrelation does not allow year to year connection (Bartsch et al. 2019). As ice content in the active layer also relates to composition, such as soil organic carbon content and soil moisture, it has been shown locally to be connected to InSAR-derived subsidence (Wu et al. 2020; Chen et al. 2020). Drained lake basins, which are usually characterized by wetter soils than their surrounding, show relatively high subsidence (e.g. Liu et al. 2014; Strozzi et al. 2018).

4 Ground Ice Melt Implications in Lowland Permafrost Regions

4.1 Mass Movements

4.1.1 Cryogenic Landslides and Solifluction

The majority of permafrost is located in lowland regions with moderate terrain. Mass movements are nevertheless abundant in these areas due to soil characteristics and local landscape morphology. Specifically the presence of massive ground ice is driving changes at the surface, specifically through thermokarst (see section 4.3). This ice can be deposits of former glaciations, e.g. moraine belts of the Laurentide ice sheet in NW Canada (Lewkowicz and Way 2019; Kokelj et al. 2017), marine terraces, which often contain tabular ground ice (e.g. Yamal peninsula in Russia, Leibman et al. (2015)) or syngenetic Yedoma deposits with massive ice wedges (Strauss et al. 2013; Andreev et al. 2009). Melting ice lenses or ice wedges at the base of the active layer may lead to ground collapse and eventually slope failure. Retrogressive thaw slumps (RTS) are a common type of cryogenic landslide (Burn and Lewkowicz 1990). Their occurrence in relation to unusually warm conditions has been described for sites in Canada (Kokelj et al. 2017; Lewkowicz and Way 2019; Ward Jones et al. 2019), Alaska (Balser et al. 2014) and in Russia (Babkina et al. 2019; Kizyakov et al. 2013; Runge et al. 2022). RTS formation leads to vegetation removal which can be monitored with satellite data. As an example, more than 4000 thaw slumps have been initiated since 1984 over an area of 70.000 km² (Lewkowicz and Way 2019), covering an area of 64 km² according to analyses of Landsat data. The vast majority of studies on mass movements in permafrost areas, especially with respect to thaw slumps, relies on landcover change detection with satellite data and visual interpretations. Tundra is in most parts of the Arctic characterized by vegetation coverage (e.g. Raynolds et al. 2019). Many disturbances result therefore in removal of vegetation and soils are exposed. As RTS are on average smaller than 2 ha, the spatial resolution of remote sensing data plays an important role in detecting these features. Recent studies have shown that Landsat can be suitable for analyses of RTS trends in remote regions (Nitze et al. 2018; Lewkowicz and Way 2019; Ward Jones et al. 2019; Runge et al. 2022). Copernicus Sentinel-2 with 10 m sampling can also capture smaller RTS as common, for example, on Yamal, Siberia (Lissak et al. 2020). Joint usage of Landsat and Sentinel-2 allows for efficient detection of events (Runge et al. 2022). Recently, new studies show the capabilities of deep learning methods in detecting RTS using PlanetScope cubesat data with a resolution of 3 m (Huang et al. 2020, 2021; Nitze et al. 2021).

Features larger than 20 ha, referred to as mega slumps, are less common but can be assessed in larger detail. Documented with satellite time series data is, for example, the Batagay mega slump in Siberia which has been potentially triggered by deforestation (Yanagiya and Furuya 2020). Thaw slumps often also occur adjacent to lakes, rivers and sea shore lines, where water bodies cause a geothermal disturbance and a frequent change of morphological gradients may trigger mass movements. These can extent into extensive retrogressive thaw slumps in unusually warm years (Babkina et al. 2019; Lewkowicz and Way 2019), which further grow upslope. Such changes are in general documented with very high-resolution satellite data and thaw slump extents derived manually (Segal et al. 2016; Kokelj et al. 2017). Sediment yield and specifically dissolved organic carbon is high in adjacent lakes (Kokelj et al. 2021), which can be captured with multispectral satellite data (Dvornikov et al. 2018).

Further features in this context are active layer detachment slides (Lewkowicz and Way 2019; Rudy et al. 2016). They are in general smaller than retrogressive thaw slumps but have similar spectral characteristics. Active layer detachment slides result in the formation of bare mineral scars (top of frozen ground) and depositional areas, where an earth mass shifts with vegetation. This leads to a shift in vegetation communities (e.g. Lantz et al. 2009). On continuous permafrost, vegetation succession starts once ground stabilizes. Certain vegetation communities establish in different parts of the geomorphological feature, depending on soil characteristics and in particular altered ground water flow (Khitun et al. 2015). The association of vegetation communities with successional stages allows to estimate the age of younger landslides and indicates the sites of possible ancient detachment. Potential monitoring with satellite data is, however, currently limited as very high spatial resolution multispectral time series would be required. Comparably small features are also solifluction lobes. Solifluction is the slow flow of saturated soil downslope, indicating that no frozen ground is present in the moving layer (Washburn 1979). Lobes are present along many slopes with vegetation coverage in periglacial environments. Movement occurs seasonally and rates are in the order of a few centimetre per year. Vegetation remains present, so they cannot be clearly distinguished through landcover from their surrounding. Areas prone to solifluction can be, however, identified by combination of terrain parameters and vegetation patterns (e.g. NDVI) from satellite data (e.g. Bartsch et al. 2008a). Movement rates can be monitored with InSAR techniques (Rouyet et al. 2019).

The assessment of the variability of mass movements in permafrost, specifically the speed at which they occur and the surface feature that they can be associated with, requires a wide range of approaches for their monitoring. Seasonality overlaps in some case with long-term change. Only slow moving features such as rock glaciers and solifluction (e.g. Barboux et al. 2014; Rouyet et al. 2019) can be quantified with repeat pass InSAR. The applicability of bistatic SAR could be demonstrated for change detection in thaw slumps, which change rapidly (Zwieback et al. 2018), but such constellations are rarely available. Alternatively, a series of InSAR-derived elevation models could be used (Bernhard et al. 2020). Repeat stereo photogrammetry and LiDAR are, however, commonly applied for local studies (Jorgensen et al. 2016). Repeat stereo photogrammetry also allowed to identify the formation of pingo-like mounds and subsequent formation of large craters on the Yamal Peninsula (approximately 80 m deep and 30 m wide; Kizyakov et al. 2015). Such features are the result of unusually warm years, which lead to the release of gas formed during the dissociation of gas hydrates, with the formation of a gas emission crater.

4.1.2 Coastal Erosion and Cliff-top Retreat

Permafrost coasts are particularly affected by rising air temperatures with rapid ground ice melt and permafrost thaw, making the coast more susceptible to erosion (Irrgang et al. 2022). Coastal erosion along the Arctic coasts occurs at rates of on average 0.5 m per year (Lantuit et al. 2012) and in some places at more than 17 m per year (Jones et al. 2018a, 2020). It poses a threat for settlements as well as archaeological sites. Irrgang et al. (2019) estimated that about 50% of cultural sites will be soon lost along the Yukon coast. Landcover change can only be partly used in an automated way to detect mass movements in case of coastal regions or riverbanks due to similarity of reflectance of shore areas. Aerial photographs, sporadic high-resolution satellite data and in some extreme cases Landsat data (30 m) are used to manually digitize coastlines and quantify their change over time. This technique allows in general only the detection of annual or decadal changes. The retrieval of coastline change from Landsat can be automatized when decadal timescales are considered (Bartsch et al. 2020a). Results need to be interpreted with care when erosion is supposed to be mapped as also submergence and isostatic rebound leads to coastline change at permafrost coasts (Boisson et al. 2020). This technique could be, however, used for circumpolar implementation. Monitoring of seasonal behaviour with optical data is impeded by frequent cloud cover. SAR could provide an alternative but the spatial resolution is limited for this purpose in case of most available sensors. Stettner et al. (2017) demonstrated, however, the utility of X-band SAR (2.35 m nominal resolution) for retrogressive thaw slumps in association with river bank erosion in the Lena Delta. The rate of about 2.5 m over three weeks barely matches the resolution of the sensors and can only be retrieved by analysing the progression over the whole season. The method is only applicable for slopes facing directly towards the sensor as the detection principle relies on the foreshortening effect of radar data. Steep slopes appear brighter and can be therefore easily distinguished from surrounding tundra and river banks. The usually wet surfaces add to the magnitude of backscatter. A further disadvantage is, however, that actual positioning of the cliff-top which requires the existence of an elevation model valid for the time of acquisition. Rates are therefore relative but can give nevertheless valuable insight into seasonality and enable the identification of driving factors in these environments. Further developments are needed to expand the use of high-resolution SAR data to further analyse coastlines, which are not facing the sensor. Bartsch et al. (2020a) extended the approach of Stettner et al. (2017) to C- and L-band, and also tested the general ability to distinguish Arctic coastal landcover from the ocean. L-band has been identified as of high value under the consideration of incidence angle variations. Future L-band missions such as NISAR (Kellogg et al. 2020) and ROSE-L (Davidson et al. 2021) are thus of high interest for monitoring of Arctic coastal erosion.

4.2 Long-term Subsidence

Subsidence observations with InSAR techniques can be used in some cases for the retrieval of continuous time series over several years. This can document the loss of ground ice and is interpreted as climate change impact. An issue is, however, signal decorrelation, which occurs stronger for shorter wavelengths. Most available long-term application studies therefore make use of L-band data, specifically the Japanese ALOS (Advanced Land Observing Satellite) missions, due to the comparably long wavelength (22.9 cm, e.g. Liu et al. 2012). But also C-band (wavelength 5.6 cm), specifically Sentinel-1, has

been demonstrated to be suitable for the retrieval of multi-annual time series in areas with limited vegetation growth (Strozzi et al. 2018; Daout et al. 2017; Fig. 4). InSAR techniques have been specifically used to monitor multi-annual thaw subsidence triggered by disturbance through fires (Liu et al. 2014; Iwahana et al. 2016; Michaelides et al. 2019; Yanagiya and Furuya 2020). Bartsch et al. (2019) describe subsidence deviations in anomalously warm years on central Yamal (Russia). Certain soils showed no difference to normal years, whereas some landscapes feature specifically high subsidence. It has been suggested that tabular ground ice at the base of the active layer causes these differences. Zwieback and Meyer (2021) confirmed such behaviour using actual ground ice in situ data for sites across the Alaskan North Slope. Altimeter have been also investigated in this context (Musket 2015), but have not shown to be suitable to detect the subtle changes typical for tundra. Current and near-future altimeter missions do not primarily target land topography applications. Uncertainties are too high to capture the majority of terrain variations related to permafrost thaw processes (Kern et al. 2020).

4.3 Lake Change

Lakes are ubiquitous landscape features, which are dotting vast swaths of remote permafrost lowlands across the Arctic. The majority of lakes on Earth are located in the northern high latitudes (Lehner and Döll 2004). Many lakes are of glacial origin but a large fraction of lakes in permafrost regions are so-called thermokarst lakes. Their formation and dynamics are closely bound to the degradation of permafrost, which is described by the thermokarst lake cycle (Grosse et al. 2013; Fig. 5). They are formed by thawing ground ice in permafrost, which creates a depression in the ground. This depression is then filled with water, e.g. from melting snow or rain. The newly developed ponds interact by slowly thawing the surrounding permafrost. Typically, this leads to expanding ponds, due to destabilizing shorelines. Over decades, centuries and millennia little thaw ponds can transform

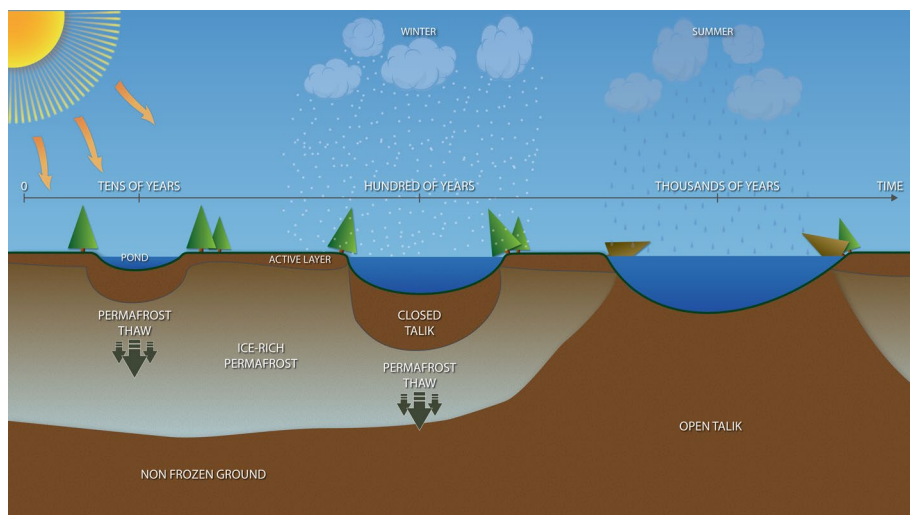


Fig. 5 Evolution of lakes through thermokarst. *Source* PAGE21—Changing permafrost in the Arctic and its Global Effects in the twenty-first century, Alfred-Wegener-Institute for Polar and Marine Research

into lakes. At the same time, permafrost beneath expanding ponds and lakes also starts to thaw and lakes are deepening over time. Thermokarst lake expansion is a self-reinforcing process. As shallow ponds and lakes ($<\sim 1.5$ m depth) are still freezing to the bottom in winter, permafrost can still be preserved beneath these ponds and lakes. However, once lake bottoms are ice-free year round, e.g. by further lake deepening or warmer and wetter winter weather, permafrost thaw beneath the lakes is accelerating (Arp et al. 2011) causing a thaw bulb, also known as talik. Permafrost thaw, particularly beneath lakes, is a source for potent greenhouse gases (e.g. carbon dioxide and methane) due to the decomposition of once freeze-locked carbon (Walter Anthony et al. 2018). Due to its sheer number and dynamic behaviour, thermokarst lakes are a significant landscape feature to monitor with remote sensing. However, thermokarst lakes are also prone to drainage. As they cannot grow infinitely, they may get drained by coalescence of lakes, tapped by rivers or the coast, overflow and create a drainage channel, or penetrate through the permafrost. Drained lakes form basins, which may retain smaller lakes and ponds or dry out completely. Due to vegetation growth, refreezing and peat accumulation, drained lake basins are typically carbon sinks, partially offsetting carbon emissions by lake expansion (Walter Anthony et al. 2018). The so-called thermokarst cycle can repeat itself across millennia and consist of several generations, which becomes apparent with multiple nested drained lake basins (Fuchs et al. 2019; Jones et al. 2022). In addition to long-term changes, thermokarst lakes also follow seasonal cycles with typically high water levels after snow melt, drying towards mid-summer and increasing lake levels in fall (Cooley et al. 2019).

Due to their abundance and importance on bio-geochemical cycles, lakes are a typical target in permafrost remote sensing. Traditionally, many studies focused on small study sites, where individual observations of aerial imagery and very high-resolution satellite data were compared to each other to analyse long-term changes (Riordan et al. 2006; Sannel and Brown 2010; Necsoiu et al. 2013; Muster et al. 2017; Jones et al. 2011). Although these approaches produce precise results, they are hardly comparable to each other, due to different sensors, spatial resolution, observation periods and limited spatial extent. In contrast to the very localized studies, coarser resolution data were used. Smith (2005) applied a large-scale analysis across different permafrost extents in NW Siberia and found clear patterns of draining lakes in discontinuous permafrost. As in other remote sensing applications, making Landsat data freely available Wulder et al. (2012) and Zhu et al. (2019) spawned many new applications including lake change analysis of thermokarst lakes. Landsat data were typically used to analyse lake changes across larger regions, such as the West Siberian lowlands (Karlsson et al. 2014), Tuktoyaktuk Peninsula in NW Canada (Olthof et al. 2015; Plug et al. 2008) or Alaska (Rover et al. 2012). All studies have in common, that lake dynamics are only analysed for a certain region, but comparable analysis capabilities across the Arctic were still lacking. With the first true global water datasets, e.g. Global Surface Water Explorer (Pekel et al. 2016) or the Aqua Monitor (Donchyts et al. 2016) it became possible to compare lake surface water changes across the Arctic. However, their accuracy in Arctic areas was highly variable, as they did not have an Arctic focus. Nitze et al. (2017) developed a lake change data product tailored to Arctic landscapes based on long-term trends of Landsat data, which was first tested in different regions in North America and Siberia and later four large transects (example subset in Fig. 6; Nitze et al. 2018). These results showed the diverse pathways and trends of lake dynamics across different regions, e.g. large lake drainage events along the boundaries of permafrost in Alaska or western Siberia. A study based on MODIS (500 m) trends concluded that surface water decline has exceeded surface water formation and expansion, leading to a net decrease in surface water since 2000 (Webb et al. 2022). Calibration and

validation for such an approach requires time series of high spatial resolution data which are still of limited availability. Satellite data have been also shown to support the automatic identification of drained lake basins (DLBs), although they can have different appearances (Bergstedt et al. 2021). The analyses of DLB patterns provide insight into past changes, before the availability of satellite data, and also supports impact assessment of drainage. Although sensors, other than optical, might be a good alternative to overcome the typical limitations in high latitude regions, e.g. clouds, low sun-angle, polar night, active sensors like SAR are rarely used for lake area extent change mapping, although lake mapping has been shown feasible in permafrost environments (Bartsch et al. 2008b; Santoro et al. 2015; Tian et al. 2016). Challenges for change mapping include emergent vegetation and sensitivity of the SAR response to wave action. Several SAR lake studies, however, focused on seasonal changes (Bartsch et al. 2012; Trofaier et al. 2013). SAR can be also applied for mapping lake ice extent and thickness (Engram et al. 2013a; Duguay and Lafleur 2003). Decreasing extent of ground fast ice over longer timescales indicates increasing temperatures (Surdu et al. 2014). Ground fast ice can be also mapped on circumpolar scale with SAR (Bartsch et al. 2017). High ground fast fraction indicates shallow lakes which are typically found on marine terraces and in Yedoma regions. Furthermore, SAR is also used to detect methane ebullition from thermokarst lakes using ice properties as proxy (Engram et al. 2013b).

Pond growth and shrinkage can be also observed in relation to ice wedge degradation. Monitoring requires very high spatial resolution time series which are rarely available. Liljedahl et al. (2016) collected suitable datasets for several sites across the Arctic and concluded that melting at the tops of ice wedges over recent decades and subsequent decimetre-scale ground subsidence is a widespread Arctic phenomenon. In general, more use of very high-resolution imagery is needed to better understand ground ice and permafrost dynamics, because permafrost degradation occurs only at the metre scale over years (Jorgensen et al. 2016).

4.4 Implications of Thaw for Carbon Fluxes

Tracking of methane and carbon dioxide in the atmosphere across the Arctic is challenging due to, for example, illumination conditions (Miner et al. 2022). Past studies using satellite data have therefore mostly focused on identification of carbon pools and mapping areas with potentially high emissions. The retrieval of active layer thickness as based on landsurface temperature integration into models (Obu 2021) may allow for the assessment of microbial activity increase with respect to permafrost thaw across the entire Arctic (Brouillette 2021). The amount of carbon stored in the soils needs to be, however, known. The representation of the heterogeneity of tundra landscapes, specifically wet versus dry, is also needed (Lara et al. 2020). Satellite records have been investigated at local to regional scale in order to identify sources of carbon (soil organic carbon, wetland distribution) through landcover mapping (e.g. Schneider et al. 2009; Hugelius et al. 2011). This is usually facilitated through optical data, but C-band SAR has been shown promising as well for regional (75 m, Reschke et al. 2012) to circumpolar retrieval with medium resolution (500 m, Widhalm et al. 2015; Bartsch et al. 2016b). More complex classifications of wetlands integrate multiple sources but provide information on comparably coarse resolution (0.5 degree; Olefeldt et al. 2021). One of the issues is that there is currently no circumpolar landcover map with sufficient spatial detail and thematic content available

to support upscaling of soil properties and fluxes (Bartsch et al. 2016a). The technical feasibility through fusion of optical and SAR data has been, however, demonstrated (ESA GlobPermafrost prototypes, 10 m; scheme applied in Bartsch et al. (2019); Bergstedt et al. (2020b)). Local InSAR subsidence patterns have been also found to represent wetness gradients (e.g. Liu et al. 2010; Strozzi et al. 2018; Bartsch et al. 2019).

Temporal dynamics based on satellite records have been so far only considered with respect to inundation which can be derived at coarse scale (fraction) based on passive microwave observations (e.g. Watts et al. 2014) and at medium resolution using indices from optical data (Webb et al. 2022). It has been also pointed out as crucial to consider different lake types for upscaling of methane emission from lakes (Matthews et al. 2020). In order to address wetting and drying processes open water fraction change, soil moisture-related information is essential. In the Arctic, the landscape heterogeneity, especially the occurrence of lakes, has so far been a major limiting factor for retrieval of near-surface soil moisture time series using microwaves (Högström and Bartsch 2017; Högström et al. 2018; Wrona et al. 2017).

5 Rock Glacier Kinematics

Mountain permafrost is widespread at all latitudes worldwide (Haeberli et al. 2010; Obu et al. 2019). The cumulative deformation of the frozen ground through long-term creep can lead to the formation of distinct tongue-shaped features of viscous flow, which are up to a kilometre wide and several kilometres long. Such features are termed rock glaciers (Haeberli 1985; Martin and Whalley 1987; Barsch 1996; Berthling 2011). The detection, mapping and monitoring of rock glaciers using remote sensing methods represents one of the most convenient and effective approaches to study mountain permafrost.

The long-term preservation of ice content under a rocky active layer enables rock glaciers to creep over long time periods (Haeberli et al. 2006; Cicora et al. 2020). Annual rates of motion of rock glaciers range from a few millimetres to several metres per year and vary within the annual cycle, from year to year, as well as at the decennial timescale (Delaloye et al. 2010; Delaloye and Staub 2016; Kaufmann and Kellerer-Pirklbauer 2015; Staub et al. 2016; Eriksen et al. 2018; PERMOS 2016). Creep rates of ice-rich frozen ground are particularly affected by climatic conditions through induced variations in the thermal conditions below freezing point, causing potential acceleration or deceleration of motion (Kääb et al. 2007; Sorg et al. 2015; Marcer et al. 2021). An increasing number of in situ studies have monitored the creep behaviour of active rock glaciers in the European Alps during the last decade (Delaloye and Staub 2016; Marcer et al. 2021; Scapozza et al. 2014; Roer et al. 2008; Stoffel and Huggel 2012). Observations showed that a majority of the surveyed rock glaciers, irrespective of their size and velocity, responded sensitively and almost synchronously to inter-annual and decennial ground temperature changes. The creep rate of rock glaciers is thus considered a valuable indicator of environmental, in particular of climatic, and ground-thermal conditions. Besides their geomorphic and climatic significance, creeping frozen sediments can also be the source of rockfall and debris flows and thus evolve into local-scale natural hazards (Deline et al. 2015; Schoeneich et al. 2014; Bodin et al. 2016; Kummert et al. 2017; Scotti et al. 2016). In addition, mountain permafrost also affects the water cycle in high mountains (Azócar and Brenning 2009).

The spatial distribution of rock glaciers is generally investigated through the use of geodatabases defined as inventories. Today, although many regional rock glacier inventories

exist, they do not provide an exhaustive and systematic worldwide coverage (Jones et al. 2018b; Brardinoni et al. 2019). Existing rock glacier inventories have various ages and have often been compiled using different methodologies. These largely depend on the availability of appropriate source data, the experience of the cartographer and potential review processes. Additionally, inventories may also differ due to varying objectives motivating each single study. Due to these factors, it is presently not possible to merge all existing inventories into a single coherent and comparable database (Jones et al. 2018b; Brardinoni et al. 2019). In order to address and overcome this issue, the IPA (International Permafrost Association) Action Group ‘Rock glacier inventories and kinematics (2018–2022)’ is developing widely accepted standard guidelines for inventorying rock glaciers on a global scale (Delaloye et al. 2018). This project is additionally motivated by the increasing emergence of open-access satellite imagery, which facilitates the development of new inventories and/or the update of existing ones.

The growing availability of remotely sensed data also enables the systematic detection of rock glacier surface motion and consequently allows the integration of kinematic information in standardized rock glacier inventories. The activity of rock glaciers cannot be determined easily using only field observations or photographs, as rock glaciers are typically composed of several superimposed units of different generations and activity levels and thus render a complex topography. Remote sensing techniques are thus key to a

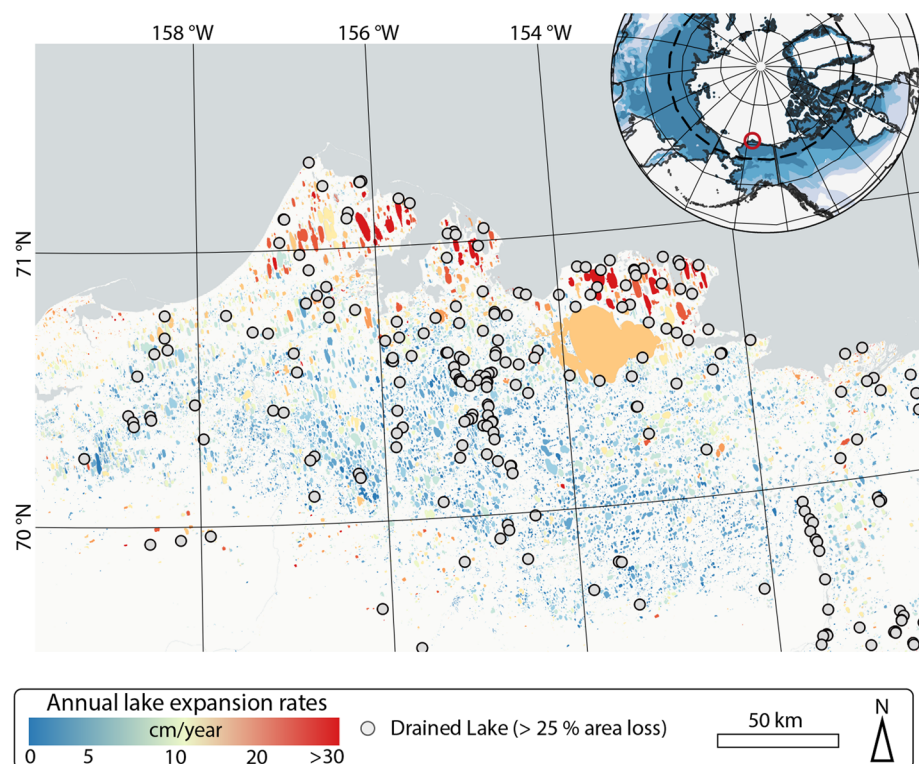


Fig. 6 Mean annual lake expansion rates on the Alaska North Slope from 1999–2014 based on lake change rates in Nitze et al. (2018). Lake expansion rates are strongly linked to changes in stratigraphy with rapid growth in the Outer Coastal Plain with very ice-rich fine-grained sediments

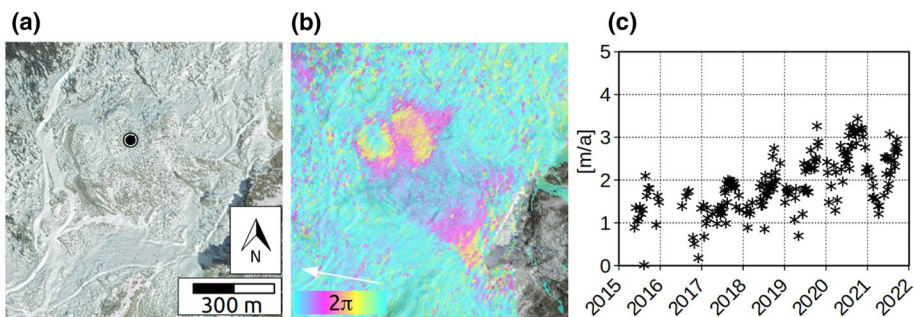


Fig. 7 Rock glacier monitoring: **a** Distelhorn rock glacier (Mittertal, Switzerland) with position of the time series (black dot), image data are from Google, DigitalGlobe. **b** Copernicus Sentinel-1 interferogram from 02.08.2018 to 08.08.2018, $2\pi \Leftrightarrow 2.8$ cm. The white arrow indicates the satellite line-of-sight. **c** Velocity along the maximum slope direction from Copernicus Sentinel-1 InSAR

better understanding of rock glacier kinematics and permafrost development. Documenting the kinematic attribute of rock glaciers and other bodies of frozen mountain sediments at regional scales is currently best done using satellite radar interferometry (Fig. 7), supported by optical and topographic data (Rignot 2002; Kenyi and Kaufmann 2003; Strozzi et al. 2004). This method enables the detection of rock glacier motion of hundreds of individual landforms over large regions. The approach has been used to develop rock glacier motion inventories for the Swiss Alps (Kenner et al. 2019); Sierra Nevada, California (Liu et al. 2013); northern Iceland (Lilleøren et al. 2013); Brooks Range, Alaska (Rick et al. 2015); Carpathians, Romania (Necsoiu et al. 2016); northeastern Tien Shan, Xinjiang, China (Wang et al. 2017), Ile Alatau and Kungöy Ala-Too, northern Tien Shan (Käab et al. 2021); and the dry Andes of Argentina and Chile (Villarroel et al. 2018). These studies mainly relied on satellite synthetic aperture radar (SAR) L-band data from the JERS-1 and PALSAR-1/2 instruments and C-band data from the ERS-1/2, ENVISAT and Sentinel-1 satellites. The categorisation of the kinematic attribute consists of semi-quantitative classes of the multi-annual downslope displacement rate of the entire rock glacier body (Delaloye et al. 2018). In a recent inventory, more than 3,600 rock glaciers have been classified according to their kinematics using InSAR worldwide (Bertone et al. 2022). A large number of fast-moving rock glaciers (i.e. with kinematic attributes of 'dm/yr to m/yr' and 'm/yr or higher') are found in the Vanoise, Central Andes and Northern Tien Shan regions.

The creep velocity of frozen debris in cold mountains is expected to increase with ground temperature (Käab et al. 2007; Arenson and Springman 2005; Arenson et al. 2015; Müller et al. 2016), although it is also influenced significantly by a number of other factors, such as the local topography, provision of ice and debris, temporal and spatial variations in ice content, rheology of the frozen debris, thickness of the creeping permafrost layer and advection, infiltration or internal production of water (Jansen and Hergarten 2006; Cicoira et al. 2019b; Kenner et al. 2019). Particularly the latter can enhance the response of creep rates of frozen debris to rising ground temperatures when approaching melting conditions (Delaloye and Staub 2016; Sorg et al. 2015; Ikeda et al. 2008; Arenson et al. 2015; Hartl et al. 2016; Buchli et al. 2018; Cicoira et al. 2019a). Because changes in rock glacier motion are believed to be an indicator of mountain permafrost conditions, there is a growing interest in their monitoring (Delaloye et al. 2018; Bertone et al. 2022). So far, most of the velocity measurements of rock glaciers are based on terrestrial geodetic surveys

(Delaloye et al. 2010; Marcer et al. 2021; Scapozza et al. 2014; Roer et al. 2008; Stoffel and Huggel 2012). This is due to the long and irregular acquisition time intervals of past SAR missions that prevented any previous worldwide monitoring of rock glacier kinematics. With the emergence of the Copernicus Sentinel-1 constellation in 2015, however, this issue was overcome, as SAR images of the same orbit are now regularly acquired every six days over Europe and every 12 days over other mountainous areas worldwide (Torres et al. 2012). Sentinel-1 InSAR can thus strongly complement worldwide in situ measurements of active rock glacier kinematics (Strozzi et al. 2020). The recent acceleration of rock glaciers at sites in Switzerland could be documented (Fig. 7). In order to retrospectively reconstruct rock glacier surface velocities at longer timescales reflecting climatic cycles (i.e. at roughly decennial timescales) and thus reaching back into the last century, other remote sensing methods such as offset tracking are employed, relying on historic and modern ground, air and satellite imagery (Scapozza et al. 2014; Kääb 2008; Kaufmann 2012; Monnier and Kinnard 2017).

6 Summary and Conclusions

Space observable parameters related to ground temperature, specifically landsurface temperature and surface status, have been shown to be applicable for circumpolar to global assessment of permafrost (Table 4), although still at limited spatial detail (1 km). Time series can be produced on global scale combining satellite records with reanalyses data and modelling heat transfer. Trend patterns can be observed which are in line with in situ observations. Northern hemisphere ground temperature changes from year to year correlate with sea ice concentrations. Land and sea cryosphere change need to be continuously jointly monitored facilitating early warning of tipping elements in the climate system. Continuity of landsurface temperature measurements needs to be ensured and improved (specifically spatial resolution) to meet science requirements.

Abrupt thaw has been identified as a regional impact tipping point at 1.5 °C over a 200-year timescale (McKay et al. 2022). Ground temperature time series need to be therefore complemented by monitoring of further local surface features which reflect abrupt thaw such as lakes and drained lake basins, thaw slumps, coastal erosion and ground subsidence (Table 4). The utility of satellite data has been proven at local to regional scale in all cases, but circumpolar implementation is still lacking. General drying (water surface loss) can be already observed across the Arctic using indices from medium resolution observations. Regional studies indicate also increasing thaw slump activities throughout the last 20 years. The use of satellite data for assessment of permafrost as a tipping element has been nevertheless so far limited (Swingedouw et al. 2020). Recent advances have been made with, e.g. the Copernicus Sentinel missions, InSAR techniques and also machine learning. However, much higher spatial resolution observations are required for detailed analysis of landscape processes in heterogeneous tundra environments. Commercial satellite data with high (e.g. PlanetScope: 3.15 m) or very high-resolution (Worldview, GeoEye: < 1 m) will further help to detect even small disturbances, but data accessibility remains limited. Although applicable SAR data are accessible through the Copernicus Sentinel-1 missions, utility remains limited due to acquisition strategies which disadvantage northern latitude permafrost regions.

Table 4 Knowledge gain on permafrost features with satellite data. *LST* Landsurface temperature, *NH* Northern hemisphere, *InSAR* Interferometry using Synthetic Aperture Radar

Feature	Approach	Information gained through satellite observations	References	Challenges
Extent of permafrost	Use of LST for permafrost modelling	The actual area underlain by permafrost (permafrost area) accounts for approximately 14 million km ² (15% of the exposed NH landsurface area), globally 13.97 km ² (10.75%)	Obu (2021) based on Obu et al. (2019)	Spatial resolution limitation for landsurface temperature (currently 1 km), adequate soil parameterization for the entire Arctic needed, unavailability of snow water equivalent at model resolution
Ground temperature trends	Use of LST for permafrost modelling	Since 2000, northern hemisphere permafrost ground temperatures (2 m) have increased on average by about one degree Celsius	This paper, based on Obu et al. (2021b)	Miner et al. (2022) based on Obu et al. (2021b) starting 1997
Active layer thickness trends	Use of LST for permafrost modelling	Deepening of on average 2.5 cm across NH during 2007–16 compared to the previous decade	Brouillette (2021), based on Obu et al. (2021a)	

Table 4 (continued)

Feature	Approach	Information gained through satellite observations	References	Challenges
Magnitude of ground subsidence	InSAR	Seasonal subsidence is in the order of several cm per year and usually higher in drained lake basins	E.g. Liu et al. (2010, 2012, 2014), Short et al. (2011)	Regional to circumpolar implementation lacking, inconsistent acquisition strategy for SAR data over northern high latitude permafrost regions
		Multi-annual subsidence has been observed at several high latitude sites	E.g. Liu et al. (2012), Strozzi et al. (2018)	
		Warmer than average summer temperatures trigger melt at the base of the active layer	Baritsch et al. (2019), Zwieback and Meyer (2021)	
		Fires trigger higher than normal subsidence	Liu et al. (2014) Iwahana et al. (2016) Michaelides et al. (2019) Yanagiya and Furuya (2020)	
Thaw lake change/ wetting versus drying	Landcover change from indices trends	Diverse pathways and trends of lake dynamics across different regions at 30 m resolution, e.g. large lake drainage events along the boundaries of permafrost in Alaska or western Siberia	Nitze et al. (2018)	Circumpolar monitoring lacking but feasible
		Over the past two decades, surface water decline has exceeded surface water formation and expansion (based on 500 m), leading to a net decrease in surface water	Webb et al. (2022)	Limited calibration and validation with high spatial resolution data across the Arctic

Table 4 (continued)

Feature	Approach	Information gained through satellite observations	References	Challenges
Ice wedge degradation	Landcover change	Melting at the tops of ice wedges over recent decades and subsequent decimetre-scale ground subsidence is a widespread Arctic phenomenon	Liljedah et al. (2016) Lewkowicz and Way (2019), Runge et al. (2022)	Circumpolar monitoring lacking due to lack of data
Thaw slump activity	Landcover change, abrupt vegetation decline	Several hundred thousand of in the last decades active thaw slumps exist across the entire Arctic, triggered by warmer than average temperatures. Increasing activities can be observed since 2000		Circumpolar monitoring lacking, issues with spatial resolution and ambiguities in the change detection
Rock glacier kinematics	InSAR	More than 3600 rock glaciers are classified according to their kinematics	Bertone et al. (2022) Strozzi et al. (2020)	Global monitoring challenging due to high manual editing effort

Carbon stored in the ground needs to be quantified in order to assess the impact of permafrost thaw on the carbon cycle. Soil saturation conditions (wetland distribution) need to be monitored in addition in this context in order to facilitate upscaling of methane emissions. Landcover has been shown as a suitable proxy at local to regional scale, but circumpolar implementation at sufficient spatial and thematic detail is still lacking.

The state of the art for documenting the kinematic attribute of rock glaciers at regional scales and monitoring the rate of motion of rock glaciers at a local scale is the use of satellite radar interferometry. However, higher spatial and temporal resolution should be considered for future missions.

Acknowledgements Sea ice concentration data from 1997 to 2019 were obtained from <https://www.meereisportal.de> (grant: REKLIM-2013-04). The info-graphic for thermokarst has been obtained from <https://page21.eu/press-center/2-uncategorised/55-promotional-material> (PAGE21, grant: 282700, funded by EC Seventh Framework Programme theme FP7-ENV-2011). Metop ASCAT FT2T retrieval (Fig. 3) was supported by C. Kroisleitner (b.geos) as well as B. Heim and M. Wieczorek (AWI).

Author Contributions All authors have equally contributed to writing of the manuscript.

Funding This work was supported by the European Space Agency CCI+ Permafrost (4000123681/18/I-NB) and Polar Science Cluster EO4PAC (4000134425/21/I-NB) projects, HGF AI-CORE, the European Research Council projects No. 885646 (PetaCARB) and 951288 (Q-Arctic), Horizon 2020 Research and Innovation Programme under Grant Agreement No. 869471 (CHARTER), ESA Polar Science Cluster community action AMPAC-Net (4000137912/22/I-DT), ESA AALM4INFRAM (4000128395/19/I-DT) and the NSF funded Permafrost Discovery Gateway (NSF Grants #2052107 and #1927872).

Data availability Not applicable.

Declarations

Conflict of interest The authors declare no conflict of interest.

Ethical approval This article does not contain any studies with human participants or animals performed by any of the authors.

Consent to participate Not applicable.

Consent for publication Not applicable.

Code availability Not applicable.

Open Access This article is licensed under a Creative Commons Attribution 4.0 International License, which permits use, sharing, adaptation, distribution and reproduction in any medium or format, as long as you give appropriate credit to the original author(s) and the source, provide a link to the Creative Commons licence, and indicate if changes were made. The images or other third party material in this article are included in the article's Creative Commons licence, unless indicated otherwise in a credit line to the material. If material is not included in the article's Creative Commons licence and your intended use is not permitted by statutory regulation or exceeds the permitted use, you will need to obtain permission directly from the copyright holder. To view a copy of this licence, visit <http://creativecommons.org/licenses/by/4.0/>.

References

André C, Ottlé C, Royer A, Maignan F (2015) Land surface temperature retrieval over circumpolar Arctic using SSM/I-SSMIS and MODIS data. *Remote Sens Environ* 162:1–10. <https://doi.org/10.1016/j.rse.2015.01.028>

Andreev AA, Grosse G, Schirrmeister L, Kuznetsova TV, Kuzmina SA, Bobrov AA, Tarasov PE, Novenko EY, Meyer H, Derevyagin AY et al (2009) Weichselian and Holocene palaeoenvironmental history of the Bol'shoy Lyakhovsky Island, New Siberian Archipelago. Arctic Siberia. *Boreas* 38(1):72–110. <https://doi.org/10.1111/j.1502-3885.2008.00039.x>

Arenson LU, Springman SM (2005) Mathematical descriptions for the behaviour of ice-rich frozen soils at temperatures close to 0 °C. *Can Geotech J* 42(2):431–442. <https://doi.org/10.1139/t04-109>

Arenson LU, Colgan W, Marshall HP (2015) Physical, thermal, and mechanical properties of snow, ice, and permafrost, snow and ice-related hazards, risks, and disasters, hazards and disasters series. Elsevier, Amsterdam. <https://doi.org/10.1016/b978-0-12-394849-6.00002-0>

Arp CD, Jones BM, Urban FE, Grosse G (2011) Hydrogeomorphic processes of thermokarst lakes with grounded-ice and floating-ice regimes on the Arctic coastal plain. *Alaska. Hydrol Process* 25(15):2422–2438. <https://doi.org/10.1002/hyp.8019>

Azócar GF, Brenning A (2009) Hydrological and geomorphological significance of rock glaciers in the dry Andes, Chile (27°–33°s). *Permafrost Periglac Process* 21(1):42–53. <https://doi.org/10.1002/ppp.669>

Babkina EA, Leibman MO, Dvornikov YA, Fakashchuk NY, Khairullin RR, Khomutov AV (2019) Activation of cryogenic processes in central yamal as a result of regional and local change in climate and thermal state of permafrost. *Russ Meteorol Hydrol* 44(4):283–290. <https://doi.org/10.3103/S1068373919040083>

Balser AW, Jones JB, Gens R (2014) Timing of retrogressive thaw slump initiation in the Noatak Basin, northwest Alaska, USA. *J Geophys Res: Earth Surf* 119(5):1106–1120. <https://doi.org/10.1002/2013JF002889>

Barboux C, Delaloye R, Lambiel C (2014) Inventorying slope movements in an alpine environment using DInSAR. *Earth Surf Process Landforms* 39(15):2087–2099. <https://doi.org/10.1002/esp.3603>

Barsch D (1996) Rockglaciers. Springer, Berlin

Bartsch A, Gude M, Gurney SD (2008a) A geomatics-based approach for the derivation of the spatial distribution of sediment transport processes in periglacial mountain environments. *Earth Surf Process Landforms* 33(14):2255–2265. <https://doi.org/10.1002/esp.1696>

Bartsch A, Pathe C, Wagner W, Scipal K (2008b) Detection of permanent open water surfaces in Central Siberia with ENVISAT ASAR wide swath data with special emphasis on the estimation of methane fluxes from Tundra Wetlands. *Hydrol Res* 39(2):89–100. <https://doi.org/10.2166/nh.2008.041>

Bartsch A, Trofai A, Hayman G, Sabel D, Schlaffer S, Clark D, Blyth E (2012) Detection of open water dynamics with ENVISAT ASAR in support of land surface modelling at high latitudes. *Biogeosciences* 9:703–714. <https://doi.org/10.5194/bg-9-703-2012>

Bartsch A, Höfler A, Kroisleitner C, Trofai A (2016a) Land cover mapping in northern high latitude permafrost regions with satellite data: achievements and remaining challenges. *Remote Sens* 8(12):979. <https://doi.org/10.3390/rs120979>

Bartsch A, Widhalm B, Kuhry P, Hugelius G, Palmtag J, Siewert M (2016b) Can C-band SAR be used to estimate soil organic carbon storage in tundra? *Biogeosciences* 13:5453–5470. <https://doi.org/10.5194/bg-13-5453-2016>

Bartsch A, Pointner G, Leibman MO, Dvornikov YA, Khomutov AV, Trofai A (2017) Circumpolar mapping of ground-fast Lake Ice. *Front Earth Sci* 5:12. <https://doi.org/10.3389/feart.2017.00012>

Bartsch A, Leibman M, Strozzi T, Khomutov A, Widhalm B, Babkina E, Mullanurov D, Ermokhina K, Kroisleitner C, Bergstedt H (2019) Seasonal progression of ground displacement identified with satellite radar interferometry and the impact of unusually warm conditions on permafrost at the Yamal Peninsula in 2016. *Remote Sens* 11(16):1865. <https://doi.org/10.3390/rs11161865>

Bartsch A, Ley S, Nitze I, Pointner G, Vieira G (2020a) Feasibility Study for the Application of Synthetic Aperture Radar for Coastal Erosion Rate Quantification Across the Arctic. *Frontiers in Environmental Science* 8:143. <https://doi.org/10.3389/fenvs.2020.00143>

Bartsch A, Matthes H, Westermann S, Heim B, Pellet C, Onaca A, Kroisleitner C, Strozzi T, Seifert FM (2020b) User requirements document—CCI+ phase 1—new ECVs—Permafrost. techreport D1.1, Gamma Remote Sensing. https://climate.esa.int/documents/684/CCI_PERMA_URD_v2.0.pdf. Accessed 4 July 2022

Bergstedt H, Bartsch A (2017) Surface state across scales; temporal and spatial patterns in land surface freeze/thaw dynamics. *Geosciences* 7:65. <https://doi.org/10.3390/geosciences7030065>

Bergstedt H, Bartsch A, Duguay CR, Jones BM (2020a) Influence of surface water on coarse resolution C-band backscatter: implications for freeze/thaw retrieval from scatterometer data. *Remote Sens Environ* 247:1111911. <https://doi.org/10.1016/j.rse.2020.1111911>

Bergstedt H, Bartsch A, Neureiter A, Hofler A, Widhalm B, Pepin N, Hjort J (2020b) Deriving a frozen area fraction from metop ASCAT backscatter based on Sentinel-1. *IEEE Trans Geosci Remote Sens* 58(9):6008–6019. <https://doi.org/10.1109/tgrs.2020.2967364>

Bergstedt H, Jones BM, Hinkel K, Farquharson L, Gaglioti BV, Parsekian AD, Kanevskiy M, Ohara N, Breen AL, Rangel RC, Grosse G, Nitze I (2021) Remote sensing-based statistical approach for defining drained lake basins in a continuous permafrost region, north slope of Alaska. *Remote Sens* 13(13):2539. <https://doi.org/10.3390/rs13132539>

Bernhard P, Zwieback S, Leinss S, Hajnsek I (2020) Mapping retrogressive thaw slumps using single-pass TanDEM-x observations. *IEEE J Sel Top Appl Earth Observ Remote Sens* 13:3263–3280. <https://doi.org/10.1109/jstars.2020.3000648>

Bertling I (2011) Beyond confusion: rock glaciers as cryo-conditioned landforms. *Geomorphology* 131(3–4):98–106. <https://doi.org/10.1016/j.geomorph.2011.05.002>

Bertone A, Barboux C, Bodin X, Bolch T, Brardinoni F, Caduff R, Christiansen HH, Darrow M, Delaloye R, Etzelmüller B, Humlum O, Lambiel C, Lilleøren KS, Mair V, Pellegrinon G, Rouyet L, Ruiz L, Strozzi T (2022) Incorporating kinematic attributes into rock glacier inventories exploiting InSAR data: preliminary results in eleven regions worldwide. *Cryosphere Discuss*. <https://doi.org/10.5194/tc-2021-342>

Biskaborn BK, Lanckman JP, Lantuit H, Elger K, Streletskiy DA, Cable WL, Romanovsky VE (2015) The new database of the Global Terrestrial Network for Permafrost (GTN-P). *Earth Syst Sci Data* 7(2):245–259. <https://doi.org/10.5194/essd-7-245-2015>

Biskaborn BK, Smith SL, Noetzli J, Matthes H, Vieira G, Streletskiy DA, Schoeneich P, Romanovsky VE, Lewkowicz AG, Abramov A, Allard M, Boike J, Cable WL, Christiansen HH, Delaloye R, Diekmann B, Drozdov D, Etzelmüller B, Grosse G, Guglielmin M, Ingeman-Nielsen T, Isaksen K, Ishikawa M, Johansson M, Johannsson H, Joo A, Kaverin D, Kholodov A, Konstantinov P, Krüger T, Lambiel C, Lanckman JP, Luo D, Malkova G, Meiklejohn I, Moskalenko N, Oliva M, Phillips M, Ramos M, Sannel ABK, Sergeev D, Seybold C, Skryabin P, Vasiliev A, Wu Q, Yoshikawa K, Zheleznyak M, Lantuit H (2019) Permafrost is warming at a global scale. *Nat Commun* 10:264. <https://doi.org/10.1038/s41467-018-08240-4>

Bodin X, Krysiecki JM, Schoeneich P, Roux OL, Lorier L, Echelard T, Peyron M, Walpersdorf A (2016) The 2006 collapse of the Bérard rock glacier (southern French Alps). *Permafrost and Periglac Process* 28(1):209–223. <https://doi.org/10.1002/ppp.1887>

Boisson A, Allard M, Sarrazin D (2020) Permafrost aggradation along the emerging eastern coast of Hudson Bay, Nunavik (northern Québec, Canada). *Permafrost Periglac Process* 31(1):128–140. <https://doi.org/10.1002/ppp.2033>

Brardinoni F, Scotti R, Sailer R, Mair V (2019) Evaluating sources of uncertainty and variability in rock glacier inventories. *Earth Surf Process Landforms* 44(12):2450–2466. <https://doi.org/10.1002/esp.4674>

Brouillette M (2021) How microbes in permafrost could trigger a massive carbon bomb. *Nature* 591(7850):360–362. <https://doi.org/10.1038/d41586-021-00659-y>

Brown J, Ferrians O, Jr, Heginbottom J, Melnikov E (1997) Circum-arctic map of permafrost and ground-ice conditions. Boulder, CO: National Snow and Ice Data Center/World Data Center for Glaciology. Digital media

Buchli T, Kos A, Limpach P, Merz K, Zhou K, Springman SM (2018) Kinematic investigations on the furggwanghorn rock glacier. Switzerland. *Permafrost Periglac Process* 29(1):3–20. <https://doi.org/10.1002/ppp.1968>

Burn C, Lewkowicz A (1990) Canadian Landform Examples—17 Retrogressive Thaw Slumps. *Canadian Geographer/Le Géographe canadien* 34(3):273–276. <https://doi.org/10.1111/j.1541-0064.1990.tb01092.x>

Chen RH, Tabatabaeenejad A, Moghaddam M (2019) Retrieval of permafrost active layer properties using time-series P-band radar observations. *IEEE Trans Geosci Remote Sens* 57(8):6037–6054. <https://doi.org/10.1109/tgrs.2019.2903935>

Chen J, Wu Y, O'Connor M, Cardenas MB, Schaefer K, Michaelides R, Kling G (2020) Active layer freeze-thaw and water storage dynamics in permafrost environments inferred from InSAR. *Remote Sens Environ* 248:112007. <https://doi.org/10.1016/j.rse.2020.112007>

Cicoira A, Beutel J, Faillietaz J, Vieli A (2019a) Water controls the seasonal rhythm of rock glacier flow. *Earth Planet Sci Lett* 528:115844. <https://doi.org/10.1016/j.epsl.2019.115844>

Cicoira A, Beutel J, Faillietaz J, Gärtner-Roer I, Vieli A (2019b) Resolving the influence of temperature forcing through heat conduction on rock glacier dynamics: a numerical modelling approach. *The Cryosphere* 13(3):927–942. <https://doi.org/10.5194/tc-13-927-2019>

Cicoira A, Marcer M, Gärtner-Roer I, Bodin X, Arenson LU, Vieli A (2020) A general theory of rock glacier creep based on in-situ and remote sensing observations. *Permafrost Periglac Process* 32(1):139–153. <https://doi.org/10.1002/ppp.2090>

Cooley SW, Smith LC, Ryan JC, Pitcher LH, Pavelsky TM (2019) Arctic-boreal lake dynamics revealed using CubeSat imagery. *Geophys Res Lett* 46(4):2111–2120. <https://doi.org/10.1029/2018GL081584>

Daout S, Doin MP, Peltzer G, Socquet A, Lasserre C (2017) Large-scale InSAR monitoring of permafrost freeze-thaw cycles on the tibetan plateau. *Geophys Res Lett* 44(2):901–909. <https://doi.org/10.1002/2016gl070781>

Davidson M, Gebert N, Giulicchi L (2021) ROSE-L—the L-band SAR mission for Copernicus. In: EUSAR 2021; 13th European conference on synthetic aperture radar, pp 1–2

Delaloye R, Lambiel C, Gärtner-Roer I (2010) Overview of rock glacier kinematics research in the Swiss Alps. *Geogr Helv* 65(2):135–145. <https://doi.org/10.5194/gh-65-135-2010>

Deline P, Gruber S, Delaloye R, Fischer L, Geertsema M, Giardino M, Hasler A, Kirkbride M, Krautblatter M, Magnin F, McColl S, Ravanel L, Schoeneich P (2015) Ice loss and slope stability in high-mountain regions, Snow and Ice-Related Hazards, Risks, and Disasters, Hazards and Disasters Series. Elsevier, Amsterdam. Pp 521–561 <https://doi.org/10.1016/b978-0-12-394849-6.00015-9>

Delaloye R, Barboux C, Bodin X, Brenning A, Hartl L, Hu Y, Ikeda A, Kaufmann V, Kellerer-Pirkbauer A, Lambiel C (2018) Rock glacier inventories and kinematics: a new IPA action group. In: Proceedings of the 5th European conference on permafrost (EUCOP5-2018), Chamonix, France

Delaloye R, Staub B (2016) Seasonal variations of rock glacier creep; time series observations from the western swiss alps. In F. Günther (Ed.), Eleventh international conference on Permafrost; exploring permafrost in a future Earth;, Volume 11, [location varies], International, pp 22. [Publisher varies]. Coordinates: N455200 N463800 E0082800 E0064800

DerkSEN C, Xu X, Dunbar RS, Colliander A, Kim Y, Kimball JS, Black TA, Euskirchen E, Langlois A, Loranty MM, Marsh P, Rautiainen K, Roy A, Royer A, Stephens J (2017) Retrieving landscape freeze/thaw state from Soil Moisture Active Passive (SMAP) radar and radiometer measurements. *Remote Sens Environ* 194:48–62. <https://doi.org/10.1016/j.rse.2017.03.007>

Donchyts G, Baart F, Winsemius H, Gorelick N, Kwadijk J, van de Giesen N (2016) Earth's surface water change over the past 30 years. *Nat Clim Change* 6(9):810–813. <https://doi.org/10.1038/nclimate3111>

Duguay CR, Lafleur PM (2003) Determining depth and ice thickness of shallow sub-Arctic lakes using space-borne optical and SAR data. *Int J Remote Sens* 24(3), 475–489. <http://dx.NOOPdoi.org/10.1080/01431160304992>

Dvornikov Y, Leibman M, Heim B, Bartsch A, Herzschuh U, Skorospekhova T, Fedorova I, Khomutov A, Widhalm B, Gubarkov A, Rößler S (2018) Terrestrial CDOM in lakes of Yamal Peninsula: connection to lake and lake catchment properties. *Remote Sens* 10(2):167. <https://doi.org/10.3390/rs10020167>

Engram M, Anthony KW, Meyer FJ, Grosse G (2013a) Characterization of L-band synthetic aperture radar (SAR) backscatter from floating and grounded thermokarst lake ice in Arctic Alaska. *The Cryosphere* 7(6):1741–1752. <https://doi.org/10.5194/tc-7-1741-2013>

Engram M, Anthony KW, Meyer FJ, Grosse G (2013b) Synthetic aperture radar (SAR) backscatter response from methane ebullition bubbles trapped by thermokarst lake ice. *Can J Remote Sens* 38(6):667–682. <https://doi.org/10.5589/m12-054>

Eriksen HØ, Rouyet L, Lauknes TR, Berthling I, Isaksen K, Hindberg H, Larsen Y, Corner GD (2018) Recent acceleration of a rock glacier complex, ádjet, Norway, documented by 62 years of remote sensing observations. *Geophys Res Lett* 45(16):8314–8323. <https://doi.org/10.1029/2018gl077605>

European Commission. Joint Research Centre (2018) User requirements for a Copernicus polar mission. Phase 1 report, User requirements and priorities. Number JRC111067. Publications Office of the European Union

Fuchs M, Lenz J, Jock S, Nitze I, Jones BM, Strauss J, Günther F, Grosse G (2019) Organic Carbon and Nitrogen Stocks Along a Thermokarst Lake Sequence in Arctic Alaska. *J Geophys Res: Biogeosci* 124(5):1230–1247. <https://doi.org/10.1029/2018JG004591>

Gangodagamage C, Rowland JC, Hubbard SS, Brumby SP, Liljedahl AK, Wainwright H, Wilson CJ, Altmann GL, Dafflon B, Peterson J, Ulrich C, Tweedie CE, Wullschleger SD (2014) Extrapolating active layer thickness measurements across arctic polygonal terrain using lidar and NDVI data sets. *Water Res Res* 50:6339–6357. <https://doi.org/10.1002/2013WR014283>

GCOS (2016) The global observing system for climate: implementation needs. Technical report GCOS-200, WMO, Geneva

GCOS (2021) The status of the global climate observing system 2021: the GCOS status report. Technical report GCOS-240, WMO, Geneva

GCOS (2022) The 2022 GCOS implementation plan. Technical Report GCOS-244, World Meteorological Organization, Geneva, Switzerland

Grosse G, Jones B, Arp C (2013) 8.21 thermokarst lakes, drainage, and drained basins. *Treatise on Geomorphology*. Elsevier, Amsterdam, pp. 325–353 <https://doi.org/10.1016/B978-0-12-374739-6.00216-5>

Hachem S, Allard M, Duguay C (2009) Using the modis land surface temperature product for mapping permafrost: an application to northern Québec and Labrador, Canada. *Permafrost and the Cryosphere* 19(1):1–12. <https://doi.org/10.1002/ppp.672>

Hachem S, Duguay CR, Allard M (2012) Comparison of MODIS-derived land surface temperatures with ground surface and air temperature measurements in continuous permafrost terrain. *The Cryosphere* 6(1):51–69. <https://doi.org/10.5194/tc-6-51-2012>

Haeberli W (1985) 01. Creep of mountain permafrost: internal structure and flow of alpine rock glaciers. *Mitteilungen der Versuchsanstalt für Wasserbau, Hydrologie und Glaziologie an der ETH Zürich* 77:5–142

Haeberli W, Hallet B, Arenson L, Elconin R, Humlum O, Kääb A, Kaufmann V, Ladanyi B, Matsuoka N, Springman S, Mühl DV (2006) Permafrost creep and rock glacier dynamics. *Permafrost and the Cryosphere* 17(3):189–214. <https://doi.org/10.1002/ppp.561>

Haeberli W, Noetzli J, Arenson L, Delaloye R, Gärtner-Roer I, Gruber S, Isaksen K, Kneisel C, Krautblatter M, Phillips M (2010) Mountain permafrost: development and challenges of a young research field. *Journal of Glaciology* 56(200):1043–1058. <https://doi.org/10.3189/002214311796406121>

Hartl L, Fischer A, Stocker-Waldhuber M, Abermann J (2016) Recent speed-up of an alpine rock glacier: an updated chronology of the kinematics of outer hochebenkar rock glacier based on geodetic measurements. *Geografiska Annaler: Series A, Physical Geography* 98(2):129–141. <https://doi.org/10.1111/geoa.12127>

Heim B, Lisovski S, Wieczorek M, Pellet C, Delaloye R, Bartsch A, Jakober D, Pointner G, Strozzi T (2021) CCI+ PHASE 1 – New ECVs Permafrost – Product Validation and Intercomparison report (PViR). techreport D4.1, Gamma Remote Sensing. https://climate.esa.int/media/documents/CCI_PERMA_PViR_v3.0_20210930.pdf. Accessed 4 Jul 2022

Högström E, Heim B, Bartsch A, Bergstedt H, Pointner G (2018) Evaluation of a MetOp ASCAT-derived surface soil moisture product in tundra environments. *Journal of Geophysical Research: Earth Surface* 123(12):3190–3205. <https://doi.org/10.1029/2018jf004658>

Högström E, Bartsch A (2017) Impact of backscatter variations over water bodies on coarse scale radar retrieved soil moisture and the potential of correcting with meteorological data. *IEEE Transactions on Geoscience and Remote Sensing* 55(1):3–13. <https://doi.org/10.1109/tgrs.2016.2530845>

Huang L, Luo J, Lin Z, Niu F, Liu L (2020) Using deep learning to map retrogressive thaw slumps in the Beiluhe region (Tibetan Plateau) from CubeSat images. *Remote Sens Environ* 237:111534. <https://doi.org/10.1016/j.rse.2019.111534>

Huang L, Liu L, Luo J, Lin Z, Niu F (2021) Automatically quantifying evolution of retrogressive thaw slumps in Beiluhe (Tibetan Plateau) from multi-temporal CubeSat images. *International Journal of Applied Earth Observation and Geoinformation* 102:102399. <https://doi.org/10.1016/j.jag.2021.102399>

Hugelius G, Virtanen T, Kaverin D, Pastukhov A, Rivkin F, Marchenko S, Romanovsky V, Kuhry P (2011) High-resolution mapping of ecosystem carbon storage and potential effects of permafrost thaw in periglacial terrain. *European Russian Arctic. Journal of Geophysical Research* 116:G03024. <https://doi.org/10.1029/2010JG001606>

Ikeda A, Matsuoka N, Kääb A (2008) Fast deformation of perennially frozen debris in a warm rock glacier in the Swiss Alps: An effect of liquid water. *Journal of Geophysical Research* 113(F1). <https://doi.org/10.1029/2007JF000859>

Irrgang AM, Lantuit H, Gordon RR, Piskor A, Manson GK (2019) Impacts of past and future coastal changes on the Yukon coast—threats for cultural sites, infrastructure, and travel routes. *Arctic Science* 5(2):107–126. <https://doi.org/10.1139/as-2017-0041>

Irrgang AM, Bendixen M, Farquharson LM, Baranskaya AV, Erikson LH, Gibbs AE, Ogorodov SA, Overduin PP, Lantuit H, Grigoriev MN, Jones BM (2022) Drivers, dynamics and impacts of changing arctic coasts. *Nature Reviews Earth and Environment* 3(1):39–54. <https://doi.org/10.1038/s43017-021-00232-1>

Iwahana G, Uchida M, Liu L, Gong W, Meyer F, Guritz R, Yamanokuchi T, Hinzman L (2016) InSAR detection and field evidence for thermokarst after a tundra wildfire, using ALOS-PALSAR. *Remote Sens* 8(3):218. <https://doi.org/10.3390/rs8030218>

Jansen, F. and S. Hergarten. 2006, Rock glacier dynamics: Stick-slip motion coupled to hydrology. *Geophys Res Lett* 33(10): n/a–n/a. <https://doi.org/10.1029/2006gl026134>

Jones BM, Grosse G, Arp CD, Jones MC, Walter Anthony KM, Romanovsky VE (2011) Modern thermokarst lake dynamics in the continuous permafrost zone, northern Seward Peninsula, Alaska. *Journal of Geophysical Research* 116:G00M03. <https://doi.org/10.1029/2011JG001666>

Jones BM, Farquharson LM, Baughman CA, Bazard RM, Arp CD, Grosse G, Bull DL, Günther F, Nitze I, Urban F, Kasper JL, Frederick JM, Thomas M, Jones C, Mota A, Dallimore S, Tweedie C, Maio

C, Mann DH, Richmond B, Gibbs A, Xiao M, Sachs T, Iwahana G, Kanevskiy M, Romanovsky VE (2018a) A decade of remotely sensed observations highlight complex processes linked to coastal permafrost bluff erosion in the Arctic. *Environ Res Lett* 13(11):115001. <https://doi.org/10.1088/1748-9326/aae471>

Jones DB, Harrison S, Anderson K, Betts RA (2018b) Mountain rock glaciers contain globally significant water stores. *Sci Rep*. <https://doi.org/10.1038/s41598-018-21244-w>

Jones BM, Irrgang AM, Farquharson LM, Lantuit H, Whalen D, Ogorodov S, Grigoriev M, Tweedie C, Gibbs AE, Strzelecki MC, Baranskaya A, Belova N, Sinitsyn A, Kroon A, Maslakov A, Vieira G, Grosse G, Overduin P, Nitze I, Maio C, Overbeck J, Bendixen M, Zagorski P, Romanovsky VE (2020) Arctic report card 2020: Coastal Permafrost Erosion. NOAA, Technical report

Jones BM, Grosse G, Farquharson LM, Roy-Léveillé P, Veremeeva A, Kanevskiy MZ, Gaglioti BV, Breen AL, Parsekian AD, Ulrich M, Hinkel KM (2022) Lake and drained lake basin systems in lowland permafrost regions. *Nat Rev Earth Environ* 3(1):85–98. <https://doi.org/10.1038/s43017-021-00238-9>

Jorgensen JC, Ward EJ, Scheuerell MD, Zabel RW (2016) Assessing spatial covariance among time series of abundance. *Ecol Evol* 6(8):2472–2485. <https://doi.org/10.1002/ece3.2031>

Kääb A (2008) Remote sensing of permafrost-related problems and hazards. *Permafrost Periglac Process* 19(2):107–136. <https://doi.org/10.1002/PPP.619>

Kääb A, Frauenfelder R, Roer I (2007) On the response of rockglacier creep to surface temperature increase. *Global Planetary Change* 56(1–2):172–187. <https://doi.org/10.1016/j.gloplacha.2006.07.005>

Kääb A, Strozzi T, Bolch T, Caduff R, Trefall H, Stoffel M, Kokarev A (2021) Inventory and changes of rock glacier creep speeds in ile Alatau and Kungöy Ala-too, Northern Tien Shan, since the 1950s. *The Cryosphere* 15(2):927–949. <https://doi.org/10.5194/tc-15-927-2021>

Karlsson J, Lyon S, Destouni G (2014) Temporal Behavior of Lake Size-Distribution in a Thawing Permafrost Landscape in Northwestern Siberia. *Remote Sens* 6(1):621–636. <https://doi.org/10.3390/rs6010621>

Kaufmann V (2012) 01. The evolution of rock glacier monitoring using terrestrial photogrammetry: the example of äusseres hochebenkar rock glacier (Austria). *Aust J Earth Sci* 105:63–77

Kaufmann V, Kellerer-Pirklbauer A (2015) Active rock glaciers in a changing environment. Geomorphometric quantification and cartographic presentation of rock glacier surface change with examples from the Hohe Tauern range, Austria., Mountain Cartography. 16 Years ICA Commission on Mountain Cartography (1999–2015), Volume 21 of Wiener Schriften zur Geographie und Kartographie. Institut für Geographie und Regionalforschung, Universität Wien, Vienna. pp 179–190

Kelley AM, Epstein HE, Walker DA (2004) Role of vegetation and climate in permafrost active layer depth in arctic tundra of Northern Alaska and Canada. *J Glaciol Climatol* 26:269–273

Kellogg K, Hoffman P, Standley S, Shaffer S, Rosen P, Edelstein W, Dunn C, Baker C, Barela P, Shen Y, Guerrero AM, Xaypraseuth P, Sagi VR, Sreekantha CV, Harinath N, Kumar R, Bhan R, Sarma CVHS (2020) NASA-ISRO synthetic aperture radar (NISAR) mission. In: 2020 IEEE aerospace conference. Big Sky, MT, USA, 2020, pp. 1–21. <https://doi.org/10.1109/AERO47225.2020.9172638>

Kenner R, Pruessner L, Beutel J, Limpach P, Phillips M (2019) How rock glacier hydrology, deformation velocities and ground temperatures interact: examples from the swiss alps. *Permafrost Periglac Process* 31(1):3–14. <https://doi.org/10.1002/PPP.2023>

Kenyi L, Kaufmann V (2003) Estimation of rock glacier surface deformation using sar interferometry data. *IEEE Trans Geosci Remote Sens* 41(6):1512–1515. <https://doi.org/10.1109/tgrs.2003.811996>

Kern M, Cullen R, Berruti B, Bouffard J, Casal T, Drinkwater MR, Gabriele A, Lecuyot A, Ludwig M, Midthassel R, Traver IN, Parrinello T, Ressler G, Andersson E, Martin-Puig C, Andersen O, Bartsch A, Farrell S, Fleury S, Gascoin S, Guillot A, Humbert A, Rinne E, Shepherd A, van den Broeke MR, Yackel J (2020) The copernicus polar ice and snow topography altimeter (CRISTAL) high-priority candidate mission. *The Cryosphere* 14(7):2235–2251. <https://doi.org/10.5194/tc-14-2235-2020>

Khitun O, Ermokhina K, Czernyadjeva I, Leibman M, Khomutov A (2015) Floristic complexes on landslides of different age in Central Yamal, West Siberian Low Arctic, Russia. *Fennia Int J Geogr* 193: 31–52. <https://doi.org/10.11143/45321>

Kim Y, Kimball JS, Zhang K, McDonald KC (2012) Satellite detection of increasing northern hemisphere non-frozen seasons from 1979 to 2008: Implications for regional vegetation growth. *Remote Sens Environ* 121:472–487. <https://doi.org/10.1016/j.rse.2012.02.014>

Kizyakov A, Zimin M, Leibman M, Pravikova N (2013) Monitoring of the rate of thermal denudation and thermal abrasion on the western coast of Kolguev Island, using high resolution satellite images. *Kriosfera Zemli* 17(4):36–47

Kizyakov AI, Sonyushkin AV, Leibman MO, Zimin MV, Khomutov AV (2015) Geomorphological conditions of the gas-emission crater and its dynamics in Central Yamal. *Earth's Cryosphere* XIX(2):15–25

Kokelj SV, Lantz TC, Tunnicliffe J, Segal R, Lacelle D (2017) Climate-driven thaw of permafrost preserved glacial landscapes, northwestern Canada. *Geology* 45(4):371–374. <https://doi.org/10.1130/G38626.1>

Kokelj SV, Kokoszka J, van der Sluijs J, Rudy ACA, Tunnicliffe J, Shakil S, Tank SE, Zolkos S (2021) Thaw-driven mass wasting couples slopes with downstream systems, and effects propagate through Arctic drainage networks. *The Cryosphere* 15(7):3059–3081. <https://doi.org/10.5194/tc-15-3059-2021>

Kroisleitner C, Bartsch A, Bergstedt H (2018) Circumpolar patterns of potential mean annual ground temperature based on surface state obtained from microwave satellite data. *The Cryosphere* 12(7):2349–2370. <https://doi.org/10.5194/tc-12-2349-2018>

Kummert M, Delaloye R, Braillard L (2017) Erosion and sediment transfer processes at the front of rapidly moving rock glaciers: Systematic observations with automatic cameras in the western swiss alps. *Permafrost Periglac Process* 29(1):21–33. <https://doi.org/10.1002/ppp.1960>

Langer M, Westermann S, Boike J (2010) Spatial and temporal variations of summer surface temperatures of wet polygonal tundra in Siberia - implications for MODIS LST based permafrost monitoring. *Remote Sens Environ* 114(9):2059–2069. <https://doi.org/10.1016/j.rse.2010.04.012>

Lantuit H, Overduin PP, Couture N, Wetterich S, Aré F, Atkinson D, Brown J, Cherkashov G, Drozdov D, Forbes DL, Graves-Gaylord A, Grigoriev M, Hubberten HW, Jordan J, Jorgenson T, Ødegård RS, Ogorodov S, Pollard WH, Rachold V, Sedenko S, Solomon S, Steenhuisen F, Streletskaia I, Vasiliev A (2012) The arctic coastal dynamics database: a new classification scheme and statistics on arctic permafrost coastlines. *Estuar Coasts* 35(2):383–400. <https://doi.org/10.1007/s12237-010-9362-6>

Lantz TC, Kokelj SV, Gergel SE, Henry GHR (2009) Relative impacts of disturbance and temperature: persistent changes in microenvironment and vegetation in retrogressive thaw slumps. *Glob Change Biol* 15(7):1664–1675. <https://doi.org/10.1111/j.1365-2486.2009.01917.x>

Lara MJ, McGuire AD, Euskirchen ES, Genet H, Yi S, Rutter R, Iversen C, Sloan V, Wullschleger SD (2020) Local-scale Arctic tundra heterogeneity affects regional-scale carbon dynamics. *Nat Commun* 11(1). <https://doi.org/10.1038/s41467-020-18768-z>

Lehner B, Döll P (2004) Development and validation of a global database of lakes, reservoirs and wetlands. *J Hydrol* 296:1–22. <https://doi.org/10.1016/j.jhydrol.2004.03.028>

Leibman M, Khomutov A, Gubarkov A, Mullanurov D, Dvornikov Y (2015) The research station “Vaskiny Dachi” Central Yamal, West Siberia, Russia—a review of 25 years of permafrost studies. *Fennia* 193(1): 3–30. <https://doi.org/10.11143/45201>

Lenton TM, Held H, Kriegler E, Hall JW, Lucht W, Rahmstorf S, Schellnhuber HJ (2008) Tipping elements in the earth's climate system. *Proc Natl Acad Sci* 105(6):1786–1793. <https://doi.org/10.1073/pnas.0705414105>

Leverington DW, Duguay CR (1996) Evaluation of three supervised classifiers in mapping 'depth to late-summer frozen ground' Central Yukon Territory. *Can J Remote Sens* 22(2). <https://doi.org/10.1080/07038992.1996.10874650>

Lewkowicz AG, Way RG (2019) Extremes of summer climate trigger thousands of thermokarst landslides in a High Arctic environment. *Nat Commun* 10(1):1329. <https://doi.org/10.1038/s41467-019-09314-7>

Liljedahl AK, Boike J, Daanen RP, Fedorov AN, Frost GV, Grosse G, Hinzman LD, Iijima Y, Jorgenson JC, Matveyeva N, Necsoiu M, Raynolds MK, Romanovsky VE, Schulla J, Tape KD, Walker DA, Wilson CJ, Yabuki H, Zona D (2016) Pan-arctic ice-wedge degradation in warming permafrost and its influence on tundra hydrology. *Nat Geosci* 9(4):312–318. <https://doi.org/10.1038/NGEO2674>

Lilleøren KS, Etzelmüller B, Gärtner-Roer I, Kääb A, Westermann S, Gudmundsson A (2013) The distribution, thermal characteristics and dynamics of permafrost in Tröllaskagi, Northern Iceland, as inferred from the distribution of rock glaciers and ice-cored moraines. *Permafrost Periglac Process* 24(4):322–335. <https://doi.org/10.1002/ppp.1792>

Lissak C, Bartsch A, De Michele M, Gomez C, Maquaire O, Raucoules D, Roulland T (2020) Remote sensing for assessing landslides and associated hazards. *Surv Geophys* 41(6):1391–1435. <https://doi.org/10.1007/s10712-020-09609-1>

Liu L, Zhang T, Wahr J (2010) InSAR measurements of surface deformation over permafrost on the North Slope of Alaska. *J Geophys Res.* <https://doi.org/10.1029/2009jf001547>

Liu L, Schaefer K, Zhang T, Wahr J (2012) Estimating 1992–2000 average active layer thickness on the Alaskan North Slope from remotely sensed surface subsidence. *Earth Surf, J Geophys Res.* <https://doi.org/10.1029/2011jf002041>

Liu L, Millar CI, Westfall RD, Zebker HA (2013) Surface motion of active rock glaciers in the Sierra Nevada, California, USA: inventory and a case study using InSAR. *The Cryosphere* 7(4):1109–1119. <https://doi.org/10.5194/tc-7-1109-2013>

Liu L, Schaefer K, Gusmeroli A, Grosse G, Jones BM, Zhang T, Parsekian AD, Zebker HA (2014) Seasonal thaw settlement at drained thermokarst lake basins, Arctic Alaska. *The Cryosphere* 8(3):815–826. <https://doi.org/10.5194/tc-8-815-2014>

Marcer M, Cicora A, Cusicanqui D, Bodin X, Echelard T, Obregon R, Schoeneich P (2021) Rock glaciers throughout the french alps accelerated and destabilised since 1990 as air temperatures increased. *Commun Earth Environ.* <https://doi.org/10.1038/s43247-021-00150-6>

Martin HE, Whalley WB (1987) Rock glaciers. *Progr Phys Geogr: Earth Environ.* 11(2):260–282. <https://doi.org/10.1177/030913338701100205>

Matthews E, Johnson MS, Genovese V, Du J, Bastviken D (2020) Methane emission from high latitude lakes: methane-centric lake classification and satellite-driven annual cycle of emissions. *Sci Rep.* <https://doi.org/10.1038/s41598-020-68246-1>

McKay DIA, Staal A, Abrams JF, Winkelmann R, Sakschewski B, Loriani S, Fetzer I, Cornell SE, Rockstrom J, Lenton TM (2022) Exceeding 1.5 degree c global warming could trigger multiple climate tipping points. *Science* <https://doi.org/10.1126/science.abn7950>

McMichael CE, Hope AS, Stow DA, Fleming JB (1997) The relation between active layer depth and a spectral vegetation index in arctic tundra landscapes of the north slope of alaska. *Int J Remote Sens* 18(11). <https://doi.org/10.1080/014311697217666>

Michaelides RJ, Schaefer K, Zebker HA, Parsekian A, Liu L, Chen J, Natali S, Ludwig S, Schaefer SR (2019) Inference of the impact of wildfire on permafrost and active layer thickness in a discontinuous permafrost region using the remotely sensed active layer thickness (ReSALT) algorithm. *Environ Res Lett* 14(3):035007. <https://doi.org/10.1088/1748-9326/aaf932>

Miner KR, Turetsky MR, Malina E, Bartsch A, Tamminen J, McGuire AD, Fix A, Sweeney C, Elder CD, Miller CE (2022) Permafrost carbon emissions in a changing arctic. *Nat Rev Earth Environ* 3(1):55–67. <https://doi.org/10.1038/43017-021-00230-3>

Monnier S, Kinnard C (2017) Pluri-decadal (1955–2014) evolution of glacier-rock glacier transitional landforms in the central andes of chile (30–33° s). *Earth Surf Dyn* 5(3):493–509. <https://doi.org/10.5194/esurf-5-493-2017>

Müller J, Vieli A, Gärtner-Roer I (2016) Rock glaciers on the run - understanding rock glacier landform evolution and recent changes from numerical flow modeling. *The Cryosphere* 10(6):2865–2886. <https://doi.org/10.5194/tc-10-2865-2016>

Muskett RR (2015) ICESat GLAS elevation changes and ALOS PALSAR InSAR line-of-sight changes on the continuous permafrost zone of the North Slope, Alaska. *Int J Geosci* 06(10):1101–1115. <https://doi.org/10.4236/ijg.2015.610086>

Muster S, Roth K, Langer M, Lange S, Cresto Aleina F, Bartsch A, Morgenstern A, Grosse G, Jones B, Sannel ABK, Sjöberg Y, Günther F, Andresen C, Veremeeva A, Lindgren PR, Bouchard F, Lara MJ, Fortier D, Charbonneau S, Virtanen TA, Hugelius G, Palmtræg J, Siewert MB, Riley WJ, Koven CD, Boike J (2017) PeRL: a circum-arctic permafrost Region Pond and Lake database. *Earth Syst Sci Data* 9(1):317–348. <https://doi.org/10.5194/essd-9-317-2017>

Naeimi V, Paulik C, Bartsch A, Wagner W, Kidd R, Park SE, Elger K, Boike J (2012) ASCAT Surface State Flag (SSF): extracting information on surface freeze/thaw conditions from backscatter data using an empirical threshold-analysis algorithm. *IEEE Trans Geosci Remote Sens* 50(7):2566–2582. <https://doi.org/10.1109/TGRS.2011.2177667>

National Research Council (2014) Opportunities to use remote sensing in understanding permafrost and related ecological characteristics: report of a workshop. National Academies Press, Washington, DC. <https://doi.org/10.17226/18711>

Necsoiu M, Dinwiddie CL, Walter GR, Larsen A, Stothoff SA (2013) Multi-temporal image analysis of historical aerial photographs and recent satellite imagery reveals evolution of water body surface area and polygonal terrain morphology in Kobuk Valley National Park. Alaska. *Environ Res Lett* 8(2):025007. <https://doi.org/10.1088/1748-9326/8/2/025007>

Necsoiu M, Onaca A, Wigginton S, Urdea P (2016) Rock glacier dynamics in southern carpathian mountains from high-resolution optical and multi-temporal SAR satellite imagery. *Remote Sens Environ* 177:21–36. <https://doi.org/10.1016/j.rse.2016.02.025>

Nelson FE, Shiklomanov NI, Mueller GR, Hinkel KM, Walker DA, Bockheim JG (1997) Estimating active-layer thickness over a large region: Kuparuk river basin, Alaska, U.S.A. *Arctic Alpine Res* 29(4). <https://doi.org/10.2307/1551985>

Nitze I, Grosse G, Jones B, Arp C, Ulrich M, Fedorov A, Veremeeva A (2017) Landsat-Based Trend Analysis of Lake Dynamics across Northern Permafrost Regions. *Remote Sens* 9(7):640. <https://doi.org/10.3390/rs9070640>

Nitze I, Grosse G, Jones BM, Romanovsky VE, Boike J (2018) Remote sensing quantifies widespread abundance of permafrost region disturbances across the Arctic and Subarctic. *Nat Commun* 9(1):5423. <https://doi.org/10.1038/s41467-018-07663-3>

Nitze I, Heidler K, Barth S, Grosse G (2021) Developing and testing a deep learning approach for mapping retrogressive thaw slumps. *Remote Sens*. <https://doi.org/10.3390/rs13214294>

Obu J (2021) How much of the Earth's surface is underlain by permafrost? *Earth Surf, J Geophys Res.* <https://doi.org/10.1029/2021jf006123>

Obu J, Westermann S, Bartsch A, Berdnikov N, Christiansen HH, Dashtseren A, Delaloye R, Elberling B, Etzelmüller B, Kholodov A, Khomutov A, Kääb A, Leibman MO, Lewkowicz AG, Panda SK, Romanovsky V, Way RG, Westergaard-Nielsen A, Wu T, Yamkhin J, Zou D (2019) Northern hemisphere permafrost map based on TTOP modelling for 2000–2016 at 1 km² scale. *Earth Sci Rev* 193:299–316. <https://doi.org/10.1016/j.earscirev.2019.04.023>

Obu J, Westermann S, Barboux C, Bartsch A, Delaloye R, Grosse G, Heim B, Hugelius G, Irrgang A, Kaab AM, Kroisleitner C, Matthes H, Nitze I, Pellet C, Seifert FM, Strozzi T, Wegmüller U, Wieczorek M, Wiesmann A (2021a) ESA Permafrost Climate Change Initiative (permafrost CCI): Permafrost active layer thickness for the Northern Hemisphere, v3.0. CEDA. <https://doi.org/10.5285/67a3f8c8dc914ef99f7f08eb0d997e23>

Obu J, Westermann S, Barboux C, Bartsch A, Delaloye R, Grosse G, Heim B, Hugelius G, Irrgang A, Kaab AM, Kroisleitner C, Matthes H, Nitze I, Pellet C, Seifert FM, Strozzi T, Wegmüller U, Wieczorek M, Wiesmann A (2021b) ESA Permafrost Climate Change Initiative (permafrost CCI): Permafrost ground temperature for the Northern Hemisphere, v3.0. CEDA. <https://doi.org/10.5285/b25d4a6174de4ac78000d034f500a268>

Olefeldt D, Hovemyr M, Kuhn MA, Bastviken D, Bohn TJ, Connolly J, Crill P, Euskirchen ES, Finkelstein SA, Genet H, Grosse G, Harris LI, Heffernan L, Helbig M, Hugelius G, Hutchins R, Juutinen S, Lara MJ, Malhotra A, Manies K, McGuire AD, Natali SM, O'Donnell JA, Parmentier FJW, Räsänen A, Schädel C, Sonnentag O, Strack M, Tank S, Treat C, Varner RK, Virtanen T, Warren RK, Watts JD (2021) The boreal–arctic wetland and lake dataset (BAWLD). *Earth Syst Sci Data* 13:5127–5149. <https://doi.org/10.5194/essd-13-5127-20210>

Olthof I, Fraser RH, Schmitt C (2015) Landsat-based mapping of thermokarst lake dynamics on the Tuktoyaktuk Coastal Plain, Northwest Territories, Canada since 1985. *Remote Sens Environ* 168:194–204. <https://doi.org/10.1016/j.rse.2015.07.001>

Park H, Yoshikawa Y, Oshima K, Kim Y, Ngo-Duc T, Kimball JS, Yang D (2016) Quantification of warming climate-induced changes in terrestrial arctic river ice thickness and phenology. *J Clim* 29(5):1733–1754. <https://doi.org/10.1175/JCLI-D-15-0569.1>

Parsekian AD, Chen RH, Michaelides RJ, Sullivan TD, Clayton LK, Huang L, Zhao Y, Wig E, Moghaddam M, Zebker H, Schaefer K (2021) Validation of permafrost active layer estimates from airborne SAR observations. *Remote Sens* 13(15):2876. <https://doi.org/10.3390/rs13152876>

Peddle DR, Franklin SE (1993) Classification of permafrost active layer depth from remotely sensed and topographic evidence. *Remote Sens Environ.* [https://doi.org/10.1016/0034-4257\(93\)90103-5](https://doi.org/10.1016/0034-4257(93)90103-5)

Pekel JF, Cottam A, Gorelick N, Belward AS (2016) High-resolution mapping of global surface water and its long-term changes. *Nature* 540(7633):418–422. <https://doi.org/10.1038/nature20584>

PERMOS (2016) Permafrost in Switzerland 2010/2011 to 2013/2014. In: Noetzli J, Luethi R, Staub B (eds) Glaciological Report (Permafrost), vol 12–15. Fribourg: Cryospheric Commission of the Swiss Academy of Sciences

Plug LJ, Walls C, Scott BM (2008) Tundra Lake changes from 1978 to 2001 on the Tuktoyaktuk Peninsula, western Canadian Arctic. *Geophys Res Lett* 35(3):L03502. <https://doi.org/10.1029/2007GL032303>

Rautiainen K, Parkkinen T, Lemmetyinen J, Schwank M, Wiesmann A, Ikonen J, Derksen C, Davydov S, Davydova A, Boike J, Langer M, Drusch M, Pulliainen J (2016) SMOS prototype algorithm for detecting autumn soil freezing. *Remote Sens Environ* 180:346–360. <https://doi.org/10.1016/j.rse.2016.01.012>

Raynolds MK, Walker DA, Balser A, Bay C, Campbell M, Cherosov MM, Daniëls FJ, Eidesen PB, Ermokhina KA, Frost GV, Jedrzejek B, Jorgenson MT, Kennedy BE, Kholod SS, Lavrinenko IA, Lavrinenko OV, Magnússon B, Matveyeva NV, Metúalemsson S, Nilsen L, Olthof I, Pospelov IN, Pospelova EB, Pouliot D, Razzhivin V, Schaeffer-Strub G, Šíbk J, Telyatnikov MY, Troeva E (2019) A raster version of the circumpolar arctic vegetation map (CAVM). *Raynolds* 232:111297. <https://doi.org/10.1016/j.rse.2019.111297>

Reschke J, Bartsch A, Schlaffer S, Schepaschenko D (2012) Capability of C-Band SAR for operational wetland monitoring at high latitudes. *Remote Sens* 4:2923–2943. <https://doi.org/10.3390/rs4102923>

Rick B, Delaloye R, Barboux C, Strozzi T (2015) Detection and inventorying of slope movements in the Brooks Range, Alaska using DInSAR: a test study. In: 68th Canadian geotechnical conference and 7th Canadian permafrost conference, Quebec

Rignot E (2002) Rock glacier surface motion in beacon valley, antarctica, from synthetic-aperture radar interferometry. *Geophys Res Lett.* <https://doi.org/10.1029/2001gl013494>

Riordan B, Verbyla D, McGuire AD (2006) Shrinking ponds in subarctic Alaska based on 1950–2002 remotely sensed images: Shrinking Ponds Across Boreal Alaska. *Biogeosci, J Geophys Res.* <https://doi.org/10.1029/2005JG000150>

Roer I, Haeberli W, Avian M, Kaufmann V, Delaloye R, Lambiel C, Kääb A (2008) Observations and considerations on destabilizing active rock glaciers in the european alps. In: 9th international conference on permafrost, fairbanks, Alaska, 29 June 2008–3 July 2008, s.n

Rouyet L, Lauknes TR, Christiansen HH, Strand SM, Larsen Y (2019) Seasonal dynamics of a permafrost landscape, Adventdalen, Svalbard, investigated by InSar. *Remote Sens Environ* 231:111236. <https://doi.org/10.1016/j.rse.2019.111236>

Rover J, Ji L, Wylie BK, Tieszen LL (2012) Establishing water body areal extent trends in interior Alaska from multi-temporal Landsat data. *Remote Sens Lett* 3(7):595–604. <https://doi.org/10.1080/01431161.2011.643507>

Rudy ACA, Lamoureux SF, Treitz P, Ewijk KV, Bonnaventure PP, Budkewitsch P (2016) Terrain controls and landscape-scale susceptibility modelling of active-layer detachments, Sabine Peninsula, Melville Island, Nunavut. *Permafrof Periglac Process* 28(1):79–91. <https://doi.org/10.1002/ppp.1900>

Runge A, Nitze I, Grosse G (2022) Remote sensing annual dynamics of rapid permafrost thaw disturbances with LandTrendr. *Remote Sens Environ* 268:112752. <https://doi.org/10.1016/j.rse.2021.112752>

Sannel ABK, Brown IA (2010) High-resolution remote sensing identification of thermokarst lake dynamics in a subarctic peat plateau complex. *Can J Remote Sens* 36(suppl1):S26–S40. <https://doi.org/10.5589/m10-010>

Santoro M, Wegmüller U, Lamarche C, Bontemps S, Defourny P, Arino O (2015) Strengths and weaknesses of multi-year envisat ASAR backscatter measurements to map permanent open water bodies at global scale. *Remote Sens Environ* 171:185–201. <https://doi.org/10.1016/j.rse.2015.10.031>

Scapozza C, Lambiel C, Bozzini C, Mari S, Conedera M (2014) Assessing the rock glacier kinematics on three different timescales: a case study from the southern swiss alps. *Earth Surf. Process. Landforms* 39(15):2056–2069. <https://doi.org/10.1002/esp.3599>

Schaefer K, Liu L, Parsekian A, Jafarov E, Chen A, Zhang T, Gusmeroli A, Panda S, Zebker HA, Schaefer T (2015) Remotely sensed active layer thickness (resalt) at barrow, alaska using interferometric synthetic aperture radar. *Remote Sens* 7(4):3735–3759. <https://doi.org/10.3390/rs70403735>

Schneider J, Grosse G, Wagner D (2009) 391. Land cover classification of tundra environments in the arctic lena delta based on landsat 7 etm+ data and its application for upscaling of methane emissions. *Remote Sens Environ* 113(2): 380. <https://doi.org/10.1016/j.rse.2008.10.013>

Schoeneich P, Bodin X, Echelard T, Kaufmann V, Kellerer-Pirkbauer A, Krysiecki JM, Lieb GK (2014) Velocity changes of rock glaciers and induced hazards. In: *Engineering geology for society and territory*. Springer, Berlin, vol 1, pp 223–227 https://doi.org/10.1007/978-3-319-09300-0_42

Schuur EAG, McGuire AD, Schadel C, Grosse G, Harden JW, Hayes DJ, Hugelius G, Koven CD, Kuhrh P, Lawrence DM, Natali SM, Olefeldt D, Romanovsky VE, Schaefer K, Turetsky MR, Treat CC, Vonk JE (2015) Climate change and the permafrost carbon feedback. *Nature* 520(7546):171–179. <https://doi.org/10.1038/nature14338>

Scotti R, Crosta GB, Villa A (2016) Destabilisation of creeping permafrost: the plator rock glacier case study (central italian alps). *Permafrof Periglac Process* 28(1):224–236. <https://doi.org/10.1002/ppp.1917>

Segal RA, Lantz TC, Kokelj SV (2016) Acceleration of thaw slump activity in glaciated landscapes of the Western Canadian Arctic. *Environ Res Lett* 11(3):034025. <https://doi.org/10.1088/1748-9326/11/3/034025>

Short N, Brisco B, Couture N, Pollard W, Murnaghan K, Budkewitsch P (2011) A comparison of TerraSAR-x, RADARSAT-2 and ALOS-PALSAR interferometry for monitoring permafrost environments, case study from herschel island, canada. *Remote Sens Environ* 115(12):3491–3506. <https://doi.org/10.1016/j.rse.2011.08.012>

Smith LC (2005) Disappearing Arctic Lakes. *Science* 308(5727):1429–1429. <https://doi.org/10.1126/science.1108142>

Soliman A, Duguay C, Saunders W, Hachem S (2012) Pan-arctic land surface temperature from modis and aatsr: product development and intercomparison. *Remote Sens* 4(12):3833–3856. <https://doi.org/10.3390/rs4123833>

Sorg A, Kääb A, Roesch A, Bigler C, Stoffel M (2015) Contrasting responses of central asian rock glaciers to global warming. *Sci Rep.* <https://doi.org/10.1038/srep08228>

Spreen G, Kaleschke L, Heygster G (2008) Sea ice remote sensing using AMSR-e 89-GHz channels. *J Geophys Res.* <https://doi.org/10.1029/2005jc003384>

Staub B, Lambiel C, Delaloye R (2016) Rock glacier creep as a thermally-driven phenomenon; a decade of interannual observations from the Swiss Alps. In: Günther F (ed), Eleventh international conference

on Permafrost; exploring permafrost in a future Earth, Volume 11 of Eleventh international conference on Permafrost; exploring permafrost in a future Earth; book of abstracts, [location varies], International, pp. 96. [publisher varies]. Document Type: Conference Paper Or Compendium Article

Stettner S, Beamish A, Bartsch A, Heim B, Grosse G, Roth A, Lantuit H (2017) Monitoring inter- and intra-seasonal dynamics of rapidly degrading ice-rich permafrost riverbanks in the Lena Delta with TerraSAR-x time series. *Remote Sens* 10(2):51. <https://doi.org/10.3390/rs10010051>

Stoffel M, Hugel C (2012) Effects of climate change on mass movements in mountain environments. *Prog Phys Geogr: Earth Environ* 36(3):421–439. <https://doi.org/10.1177/030913312441010>

Strauss J, Schirrmeister L, Grosse G, Wetterich S, Ulrich M, Herzschuh U, Hubberten H (2013) The deep permafrost carbon pool of the Yedoma region in Siberia and Alaska. *Geophys Res Lett* 40(23):6165–6170. <https://doi.org/10.1002/2013GL058088>

Strozzi T, Kääb A, Frauenfelder R (2004) Detecting and quantifying mountain permafrost creep from in situ inventory, space-borne radar interferometry and airborne digital photogrammetry. *Int J Remote Sens* 25(15):2919–2931. <https://doi.org/10.1080/0143116042000192330>

Strozzi T, Antonova S, Günther F, Mätzler E, Vieira G, Wegmüller U, Westermann S, Bartsch A (2018) Sentinel-1 SAR interferometry for surface deformation monitoring in low-land permafrost areas. *Remote Sens* 10(9):1360. <https://doi.org/10.3390/rs10091360>

Strozzi T, Caduff R, Jones N, Barboux C, Delaloye R, Bodin X, Kääb A, Mätzler E, Schrott L (2020) Monitoring rock glacier kinematics with satellite synthetic aperture radar. *Remote Sens* 12(3):559. <https://doi.org/10.3390/rs12030559>

Surdu CM, Duguay CR, Brown LC, Fernández Prieto D (2014) Response of ice cover on shallow lakes of the North Slope of Alaska to contemporary climate conditions (1950–2011): radar remote-sensing and numerical modeling data analysis. *The Cryosphere* 8:167–180. <https://doi.org/10.5194/tc-8-167-2014>

Swingedouw D, Ifejika Speranza C, Bartsch A, Durand G, Jamet C, Beaugrand G, Conversi A (2020) Early warning from space for a few key tipping points in physical, biological, and social-ecological systems. *Surv Geophys* 41(6):1237–1284. <https://doi.org/10.1007/s10712-020-09604-6>

Tian B, Li Z, Tang P, Zou P, Zhang M, Niu F (2016) Use of Intensity and Coherence of X-Band SAR Data to Map Thermokarst Lakes on the Northern Tibetan Plateau. *IEEE J Sel Top Appl Earth Observ Remote Sens* 9(7):3164–3176. <https://doi.org/10.1109/JSTARS.2016.2549740>

Torres R, Snoeij P, Geudtner D, Bibby D, Davidson M, Attema E, Potin P, Rommen B, Flouri N, Brown M, Traver IN, Deghaye P, Duesmann B, Rosich B, Miranda N, Bruno C, L'Abbate M, Croci R, Pietropaolo A, Huchler M, Rostan F (2012) GMES Sentinel-1 mission. *Remote Sens Environ* 120:9–24. <https://doi.org/10.1016/j.rse.2011.05.028>

Trofaijer AM, Bartsch A, Rees WG, Leibman MO (2013) Assessment of spring floods and surface water extent over the Yamalo-Nenets autonomous district. *Environ Res Lett* 8(4):045026. <https://doi.org/10.1088/1748-9326/8/4/045026>

Trofaijer AM, Westermann S, Bartsch A (2017) Progress in space-borne studies of permafrost for climate science: towards a multi-ECV approach. *Remote Sens Environ* 203:55–70. <https://doi.org/10.1016/j.rse.2017.05.021>

Van Everdingen RO, Association IP, others (1998) Multi-language glossary of permafrost and related ground-ice terms in Chinese, English, French, German. Arctic Inst. of North America University of Calgary

Villarroel C, Beliveau GT, Forte A, Monserrat O, Morville M (2018) DInSAR for a regional inventory of active rock glaciers in the dry Andes mountains of Argentina and Chile with Sentinel-1 data. *Remote Sens* 10(10):1588. <https://doi.org/10.3390/rs10101588>

Walter Anthony K, Schneider von Deimling T, Nitze I, Frolking S, Emond A, Daanen R, Anthony P, Lindgren P, Jones B, Grosse G (2018) 21st-century modeled permafrost carbon emissions accelerated by abrupt thaw beneath lakes. *Nature Communications* 9(1):3262. <https://doi.org/10.1038/s41467-018-05738-9>

Wang L, Marzahn P, Bernier M, Jacome A, Poulin J, Ludwig R (2017) Comparison of TerraSAR-x and ALOS PALSAR differential interferometry with multisource DEMs for monitoring ground displacement in a discontinuous permafrost region. *IEEE J Sel Top Appl Earth Observ Remote Sens* 10(9):4074–4093. <https://doi.org/10.1109/jstars.2017.2707337>

Wang C, Zhang Z, Zhang H, Zhang B, Tang Y, Wu Q (2018) Active layer thickness retrieval of qinghai-tibet permafrost using the TerraSAR-x InSAR technique. *IEEE J Sel Top Appl Earth Observ Remote Sens* 11(11):4403–4413. <https://doi.org/10.1109/jstars.2018.2873219>

Ward Jones MK, Pollard WH, Jones BM (2019) Rapid initialization of retrogressive thaw slumps in the Canadian high Arctic and their response to climate and terrain factors. *Environ Res Lett* 14(5):055006. <https://doi.org/10.1088/1748-9326/ab12fd>

Washburn AL (1979) Geocryology: a survey of periglacial processes and environments. Edward Arnold, London

Watts JD, Kimball JS, Bartsch A, McDonald KC (2014) Surface water inundation in the boreal-Arctic: potential impacts on regional methane emissions. *Environ Res Lett* 9(7):075001. <https://doi.org/10.1088/1748-9326/9/7/075001>

Webb EE, Liljedahl AK, Cordeiro JA, Loranty MM, Witharana C, Lichstein JW (2022) Permafrost thaw drives surface water decline across lake-rich regions of the Arctic. *Nat Clim Change* 12(9):841–846. <https://doi.org/10.1038/s41558-022-01455-w>

Westermann S, Østby T, Gisnås K, Schuler T, Etzelmüller B (2015) A ground temperature map of the north Atlantic permafrost region based on remote sensing and reanalysis data. *The Cryosphere* 9(3):1303–1319. <https://doi.org/10.5194/tc-9-1303-2015>

Westermann S, Peter M, Langer M, Schwamborn G, Schirrmüller L, Etzelmüller B, Boike J (2017) Transient modeling of the ground thermal conditions using satellite data in the Lena river delta. *Siberia. Cryosphere* 11(3):1441–1463. <https://doi.org/10.5194/tc-11-1441-2017>

Widhalm B, Bartsch A, Heim B (2015) A novel approach for the characterization of tundra wetland regions with c-band sar satellite data. *Int J Remote Sens* 36(22):5537–5556. <https://doi.org/10.1080/01431612.2015.1101505>

Widhalm B, Bartsch A, Siewert MB, Hugelius G, Elberling B, Leibman M, Dvornikov Y, Khomutov A (2016) Site scale wetness classification of tundra regions with C-band SAR satellite data. In: *Proceedings of the ESA Living Planet Symposium*, Prague, Czech Republic, Number ESA SP-740

Widhalm B, Bartsch A, Leibman M, Khomutov A (2017) Active-layer thickness estimation from X-band SAR backscatter intensity. *The Cryosphere* 11(1):483–496. <https://doi.org/10.5194/tc-11-483-2017>

Wrona E, Rowlandson TL, Nambiar M, Berg AA, Colliander A, Marsh P (2017) Validation of the soil moisture active passive (SMAP) satellite soil moisture retrieval in an arctic tundra environment. *Geophys Res Lett* 44(9):4152–4158. <https://doi.org/10.1002/2017gl072946>

Wu Y, Chen J, O'Connor M, Ferencz SB, Kling GW, Carden MB (2020) Monitoring soil water and organic carbon storage patterns at the Arctic Foothills, Alaska, using InSar. In: *IGARSS 2020—2020 IEEE international geoscience and remote sensing symposium*. IEEE. <https://doi.org/10.1109/IGARS39084.2020.9323122>

Wulder MA, Masek JG, Cohen WB, Loveland TR, Woodcock CE (2012) Opening the archive: How free data has enabled the science and monitoring promise of Landsat. *Remote Sens Environ* 122:2–10. <https://doi.org/10.1016/j.rse.2012.01.010>

Yanagiya K, Furuya M (2020) Post-wildfire surface deformation near Batagay, eastern Siberia, detected by L-Band and C-Band InSAR. *J Geophys Res: Earth Surf* 125(7). <https://doi.org/10.1029/2019jf005473>

Zhang C, Douglas TA, Anderson JE (2021) Modeling and mapping permafrost active layer thickness using field measurements and remote sensing techniques. *Int J Appl Earth Observ Geoinform* 102:102455. <https://doi.org/10.1016/j.jag.2021.102455>

Zhao R, Wei Li Z, Cai Feng G, Jie Wang Q, Hu J (2016) Monitoring surface deformation over permafrost with an improved SBAS-InSAR algorithm: With emphasis on climatic factors modeling. *Remote Sens Environ* 184:276–287. <https://doi.org/10.1016/j.rse.2016.07.019>

Zhu Z, Wulder MA, Roy DP, Woodcock CE, Hansen MC, Radeloff VC, Healey SP, Schaaf C, Hostert P, Strobl P, Pekel JF, Lymburner L, Pahlevan N, Scambos TA (2019) Benefits of the free and open Landsat data policy. *Remote Sens Environ* 224:382–385. <https://doi.org/10.1016/j.rse.2019.02.016>

Zwieback S, Meyer FJ (2021) Top-of-permafrost ground ice indicated by remotely sensed late-season subsidence. *The Cryosphere* 15(4):2041–2055. <https://doi.org/10.5194/tc-15-2041-2021>

Zwieback S, Kokelj SV, Günther F, Boike J, Grosse G, Hajnsek I (2018) Sub-seasonal thaw slump mass wasting is not consistently energy limited at the landscape scale. *The Cryosphere* 12(2):549–564. <https://doi.org/10.5194/tc-12-549-2018>

Publisher's Note Springer Nature remains neutral with regard to jurisdictional claims in published maps and institutional affiliations.